Mineralium Deposita
https://doi.org/10.1007/s00126-024-01267-2

ARTICLE

The role of hydrothermal processes and the formation of the J-M reef and associated rocks of olivine-bearing zone I of the Stillwater Complex, Montana

A. R. Gupta[1] · **Alan E. Boudreau**[1]

Received: 24 October 2023 / Accepted: 12 April 2024

Abstract
Several lines of evidence, including hydrous melt inclusions and unusually Cl-rich apatite, have been used to suggest that the reappearance of olivine and PGE-sulfide of the J-M Reef in the Stillwater Complex, Montana, is due to fluid infiltration and hydration melting. This study builds upon the hydration melting model using the programs MELTS and PELE with Stillwater bulk rock compositions for the original protolith. Cl-bearing phases are not modeled by MELTS and thus simple oxide mixtures of either a pure H_2O or a $H_2O + Na_2O$ "faux brine" are added to norite, gabbronorite, and melanorite protoliths at 1050 °C at 2 kbar pressure, conditions for which the nominally "dry" protolith is > 95% solid. Incongruent hydration melting results in up to 37% olivine produced in the melanorite. The olivine Fo content is a function of the partial melt retained on cooling, and ranges between 76 and 86, overlapping the natural range of olivine compositions observed in the rocks. Modeling with the PELE program, which includes a silicate liquid Cl component, sulfur species, and a more complex C-O–H-S fluid, suggests that, for CO_2-rich fluids, fluid metal concentrations on the order of 25 ppm Pt, 75 ppm Pd, 0.03 wt.% Cu, and 0.20 wt.% Ni at a fluid/rock mass ratio of ~ 0.25 are needed to account for the observed ore grades. Sulfide and ore metals are readily remobilized for more H_2O-rich fluids, consistent with heterogeneous distribution of sulfide and regionally variable ore grades.

Keywords Platinum-group elements · Hydration melting · Stillwater Complex · J-M Reef

Introduction

A wide variety of processes have been proposed to explain the features observed in layered igneous intrusions, ranging from conventional to the unusual and controversial (Latypov et al. 2023). This is particularly true for the debate over the origin of platinum-group element (PGE) deposits in intrusions such as the Bushveld Complex and Stillwater Complexes, with models ranging from strictly orthomagmatic crystallization processes to those that propose magmatic volatile fluids played a significant role. (In this report, the terms "liquid" and "melt" will refer to a silicate liquid, "sulfide liquid" to an immiscible sulfide liquid, and "fluid" or "vapor" will refer to any volatile-rich, C-O–H-S-Cl-X solution.)

The main PGE deposit of the Stillwater Complex, the J-M Reef, is associated with the relatively abundant sulfide and the reappearance of olivine and sporadic chromite in the stratigraphic sequence. Petrographic models include a variety of strictly magmatic interpretations involving magma becoming oversaturated in these phases either by the introduction of a more primitive magma or a magma mixing event, to suggestions of extensive incongruent melting of floor rocks by superheated magma (e.g., Irvine et al. 1983; Barnes and Naldrett 1986; Keays et al. 2012; Jenkins et al. 2021). At the other extreme are models that suggest that the ore component was introduced by a high temperature hydrothermal fluid and that olivine and chromite were the result of incongruent melting of preexisting noritic and gabbronoritic rocks driven volatile fluxing (e.g., Boudreau 1988, 1999a). Others have suggested the involvement in both orthomagmatic and hydrothermal processes in which

Editorial handling: W. D. Maier

✉ Alan E. Boudreau
boudreau@duke.edu

[1] Division of Earth and Climate Sciences, Nicholas School of the Environment, Duke University, Durham, NC 27708, USA

Published online: 07 May 2024

the latter upgraded or otherwise modified an originally magmatic assemblage (e.g., Barnes and Campbell 1988; Godel and Barnes 2008).

This work expands the earlier work of Boudreau et al. (1986), and Boudreau (1988, 1999a) that suggests that the reappearance of olivine and chromite as well as PGE-sulfide to form the J-M Reef occurs due to the influx of a Cl-rich mineralizing fluid and resultant incongruent partial melting. Specifically, the effects of volatile fluid fluxing on Stillwater protoliths with variable amounts of pyroxene and plagioclase are modeled with the programs MELTS and PELE to reproduce the observed sulfide- and olivine-bearing rocks. It is shown that mineral compositions and modal abundances are best modeled by a brine (liberally defined) fluxing agent better than a pure H_2O fluid. Sulfide precipitation and ore grade is best modeled by a CO_2- and alkali-rich fluid over a more H_2O-rich brine. Limitations of the models illustrate the need for additional experimental work at the upper crustal conditions appropriate to high temperature hydrothermal fluids in mafic igneous systems.

Geology of the Stillwater Complex

The 2.7-billion-year Stillwater Complex is a layered ultramafic–mafic intrusion that sits on the northern edge of the Beartooth Range, a major exposed block of the Wyoming Archean Province (McCallum 2011, Wall et al. 2018 and references therein) (Fig. 1a). Its maximum exposed stratigraphic thickness is 6.5 km with an exposed strike length of about 45 km. There is some debate over the emplacement time, with Latypov (2019) disputing the contention of Wall et al. (2018) that zircon ages imply extensive out-of-sequence emplacement over several million years. Underneath the complex is a variety of rocks: the central and western part is underlined by 3270 Ma meta-volcaniclastic shales, breccia, banded iron formation as well as granite gneiss whereas to the east there is a quartz monzonite. Intrusion of Stillwater magmas resulted in a wide metamorphic aureole, whose true thickness remains uncertain due to absences of lateral continuity of rock units and extensive faulting (e.g., Labotka and Kath 2001; Thomson 2008). The upper portion of the intrusion eroded before the mid-Cambrian and was covered by Paleozoic and Mesozoic sediments. Regional faulting, thrusting, and uplift during the Late Cretaceous Laramide orogeny has led to the current moderately to steeply dipping to the NNE (and locally overturned) exposure along the northern edge to the Beartooth Plateau.

The Stillwater Complex itself has been divided into three main units – the Basal series (composed mainly of norite and orthopyroxenite), the Ultramafic series (composed of a lower olivine-bearing Peridotite zone and an upper Bronzitite zone), and the Banded series, the base of which is where plagioclase again becomes a major idiomorphic mineral. The Banded series is further divided into the Lower, Middle, and Upper Banded series, each containing additional zones and subzones based on the rock type and for which the boundaries and names differ between different investigators. The terminology and divisions shown in Fig. 1b is that suggested by Boudreau (2016). The Johns-Manville (J-M) Reef is a world-class platinum-group element (PGE) deposit defined by sulfide-enriched rocks associated with Olivine-Bearing zone I (OB-I) of the Lower Banded series. It is the character of the OB-I and its host zone, the Lower Banded series, that are explored in more detail here.

The lower banded series, olivine-bearing zone I (OB-I), and the J-M reef

At the base of the Lower Banded series and just above the contact with the Ultramafic series, pegmatoids and modal layering are typically present in Norite zone I (N-I). Above this, N-I is for the most part a texturally and modally uniform norite (McCallum et al. 1980). N-I is overlain by an initially uniform gabbronorite of Gabbronorite zone I, (GN-I) that becomes more modally layered upward. From the Bronzitite zone of the Ultramafic series up through GN-I, the rocks record an apparent crystallization sequence of orthopyroxene → orthopyroxene + plagioclase → orthopyroxene + plagioclase + augite. This is accompanied by a modestly variable but persistent decrease in Mg# of the pyroxene and in the An content of plagioclase (McCallum et al. 1980; Todd et al. 1982; Jenkins et al. 2021).

Also occurring below OB-I are a variety of discordant pegmatoids, some of which are enriched in sulfide and the PGE (Braun et al. 1994; McIlveen 1996; Zientek et al 2002; data available in Barnes et al. 2020). Although not reported from the mineralized pegmatoids, they can contain a variety of fluid inclusions, ranging from H_2O- to CO_2-rich. Salinity ranges from brines to presumably once molten halite and can occur with up to 16 inclusion minerals and contain ppm levels of Pt and Pd and with maximum estimated formation temperatures of 700–715 °C (Hanley et al. 2005, 2008).

This sequence is interrupted by OB-I where troctolites and more olivine-rich rocks occur. OB-I is variable in terms of its stratigraphic location, thickness and minerology; the Frog Pond section, south of Contact Mountain Shown in Fig. 1b, can be considered the type section which can be compared to lateral variations and occurs about 400 m above the base of the Banded series. In the lower Gabbronorite subzone of OB-I, rocks are primarily norite and gabbronorite but have minor interlayered anorthosite and a variety of heterolithic and vari-textured olivine-bearing rocks. Locally, the olivine-rich rocks can form apophyses into the overlying anorthosite (Boudreau 1988) and small pods of olivine-rich

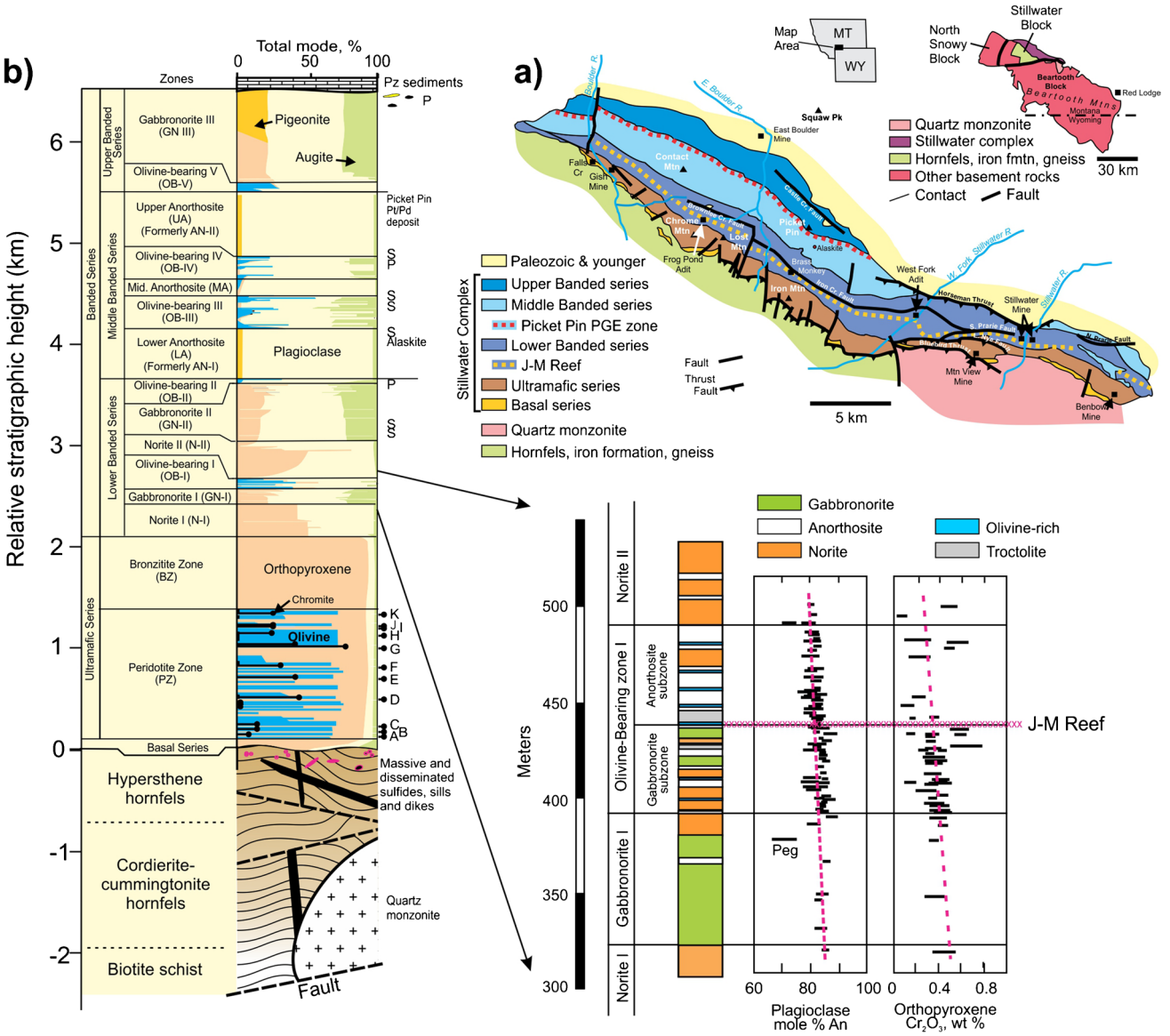

Fig. 1 **A** Location map and simplified geology of the Stillwater Complex. **B** Stillwater stratigraphic nomenclatures used in this study and modal mineralogy (after Boudreau 2016), with detail of stratigraphy with plagioclase and orthopyroxene composition trends through Olivine-Bearing Zone I (modified after Todd et al. 1982)

rock are host by underlying anorthositic rocks (Jenkins et al. 2022).

In the report, any plagioclase-poor, olivine and pyroxene-rich compositions are informally referred to as peridotites, those composed of abundant plagioclase and olivine as troctolites, and the olivine-free rocks as norites and gabbronorites with modifiers melano- or leuco- as necessary. Formal rock names otherwise can be a bit of a mouthful and somewhat misleading. Based on normative mineralogy and texture (Fig. 2 and Table 1, analysis 5), the average of the more olivine-rich would be classified as a pegmatoidal poikilitic olivine norite. They have been conventionally called an olivine meso- to orthocumulate based on the apparent extensive peritectic reaction relationship of olivine with residual liquid (e.g., Barnes and Naldrett 1986). Others note the low incompatible element content and suggest that olivine and orthopyroxene are instead cotectic minerals forming a heteradcumulate (e.g., Jenkins et al. 2021). Plagioclase, where not interstitial, can be rounded/embayed and reversely zoned in the more olivine-rich rocks (Barnes and Naldrett 1986).

Locally, layering is not laterally continuous; pothole-like terminations can occur with olivine bearing rocks against gabbronorite or anorthosites against norite and gabbronorites. On larger regional scales, OB-I and the Reef can occur at lower stratigraphic levels, with a much-thinned OB-I transitioning directly from N-I between the

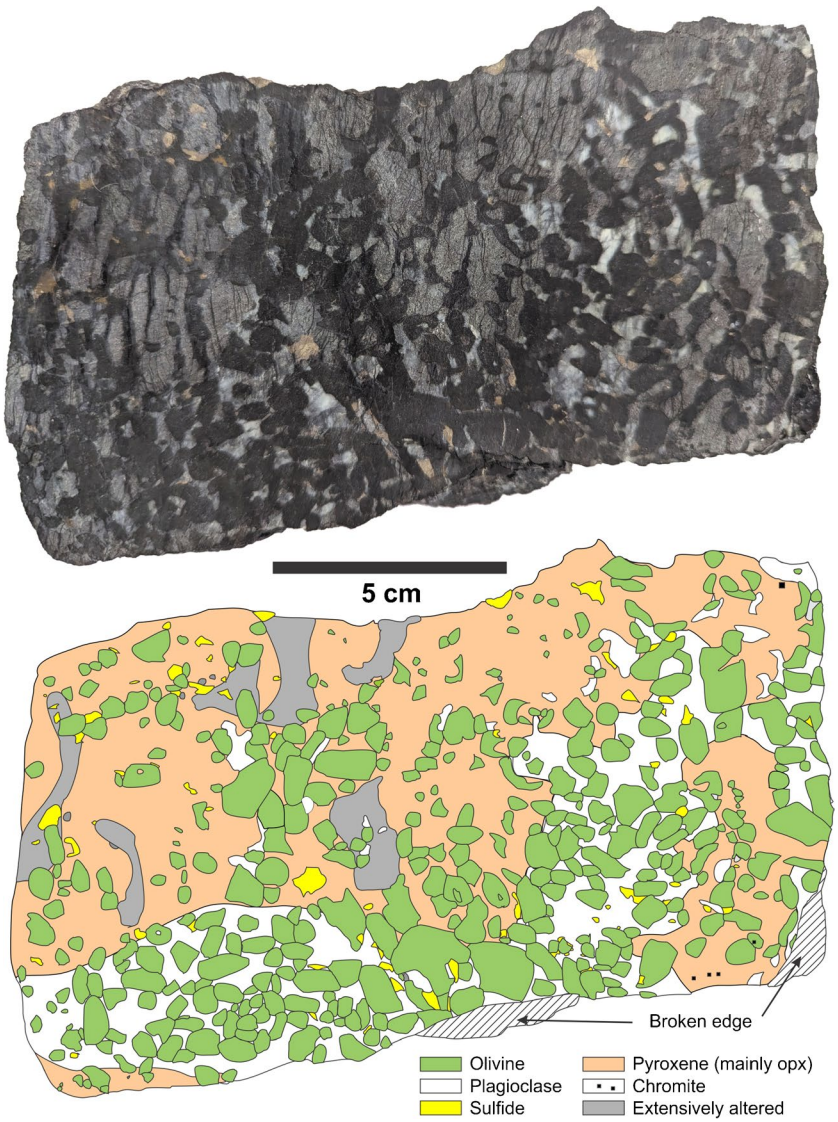

Fig. 2 Example of a mineralized pegmatitic poikilitic plagioclase harzburgite from OB-I. Minor alteration and veining removed from the lower trace drawing, except where original mineralogy is obscured

Stillwater River and East Fork of the Stillwater River in what Sibanye-Stillwater mine geologists term the "Dow Depression" (Boudreau et al. 2019; Jenkins et al. 2020).

The PGE-enriched sulfides of the J-M Reef are most common below and along the contact of the Gabbronorite and Anorthosite subzones where it is associated with olivine-rich rocks. The average grade is 18.86 ppm palladium and platinum with a palladium to platinum ratio of 3.4 to 1 over 1.4 m (Zientek et al. 2002; but see also Jenkins et al. 2020). The ore zone is not uniformly mineralized; any given mining face will have patches containing several percent sulfide surrounded by rock with very little. The metal concentrations in sulfide report by Barnes and Naldrett (1985) of 9.3 wt.% Ni, 6.9 wt.% Cu, 5440 ppm Pd and 1560 ppm Pt imply an average sulfide concentration of 0.26 wt.%. Using just bulk rock Pd content but a more extensive dataset, Barnes et al. (2020) calculate a sulfide concentration > 1wt.%. Furthermore, sulfide mineralization is typically heterogeneously distributed along the J-M reef, so much so that efficient mining requires drilling at ~ 15 m centers to define economic concentrations where sulfide can reach several percent, and locally can be concentrated in decimeter-sized bodies of massive sulfide in the cores of gabbronorite pegmatoids. Although much of the sulfide-bearing rocks occurs within a 1–3 m thick peridotite/harzburgite, locally it can extend to several tens of meters into the footwall in regions mining geologist term "ballrooms" that can extend across modal layering. Disseminated mineralization can also occur with isolated pods of olivine-bearing rocks hosted in the footwall (gabbro)norites (e.g., Zientek et al. 2002; Harper 2004). In contrast, mineralization is particularly poor and locally absent in the region of the Dow Depression noted above.

In addition to the local discontinuous nature of sulfide mineralization, there are pronounced regional east–west

Table 1 Representative average major element compositions of rocks from Olivine-Bearing zone I of the Stillwater Complex

	1 Norite	2 Gabbronorite	3 Melanorite	4 Troctolite	5 Peridotite
Major Elements:					
SiO_2 (wt.%)	48.91	50.10	53.81	46.37	41.35
TiO_2	0.11	0.10	0.14	0.07	0.12
Al_2O_3	23.68	17.12	8.47	25.95	5.54
FeO(total)	4.71	4.62	8.50	4.65	14.80
MnO	0.09	0.11	0.18	0.07	0.18
MgO	7.34	11.51	21.81	6.88	30.60
CaO	13.57	15.44	6.62	14.45	5.03
Na_2O	1.50	0.93	0.42	1.47	0.19
K_2O	0.08	0.05	0.04	0.07	0.04
P_2O_5	0.01	0.01	0.01	0.01	0.01
H_2O	0.01	0.01	0.01	0.01	0.01
Total	100.00	100.00	100.00	100.00	100.00
CIPW norm:					
or	0.5	0.3	0.2	0.4	0.2
ab	12.7	7.9	3.6	12.4	1.6
an	57.7	42.4	21.1	64.0	14.2
di	7.8	27.3	9.3	6.2	8.6
hy	16.0	16.3	65.3	1.3	14.5
ol	5.2	5.6	0.2	15.5	59.4
il	0.21	0.19	0.27	0.13	0.23
ap	0.02	0.02	0.02	0.02	0.02
or + ab + an	70.8	50.6	24.9	76.9	16.0
mg#	73.6	81.6	82.0	72.5	78.6
An	81.1	83.6	84.8	82.9	89.2

Notes: Average values of the following samples from Jenkins et al. (2021): Norite: 40,933–210, 40,933–212.7, 40,933–217, 40,933–225.4. Gabbronorite: 40,933–93.3, 40,933–9740933-101, 40,933–106.5. Troctolite: 40,933–135.2, 40,933–138.1, 40,933–139.3, 40,933–143.6. Peridotite/harzburgite (described as pegmatitic dunite samples of Jenkins et al.): 40,933–125.1, 40,933–126, 40,933–127.6, 40,933–130.5, 40,933–131.7, 40,933–132.2, 40,933–146.7. The melanorite is from Barnes et al. (2020), sample ST-05. All samples have 0.01 wt.% each of P_2O_5 and H_2O to allow possible apatite saturation of the initial bulk composition

variations in ore grades. This variation mainly occurs in the sulfur and base metal concentrations with PGE grades being less variable (Boudreau et al. 2019; Jenkins et al. 2020). Some of the variation in estimated bulk sulfide concentration noted above may reflect these regional differences. This is contrary to standard R-factor (mass silicate liquid/sulfide liquid mass ratio) explanations that predict base metals should be less variable as they saturate at relatively small amounts of magma relative to the PGE (e.g., Campbell and Naldrett 1979).

Minor disseminated chromite is sporadically observed in the more olivine-rich rocks and more rarely as concordant and discordant chromitite seams (Boudreau 1988; Waters and Boudreau 1996; Marsh et al. 2021). Polymineralic inclusions are common in chromite, chlorapatite, and olivine, although those in the latter are obscured by partial alteration of olivine to serpentine + magnetite. The inclusion assemblage typically includes abundant biotite and a pargasitic (Na-rich) amphibole (e.g., Boudreau et al. 1986). They have been interpreted to have crystallized from a volatile-rich trapped silicate liquid. The upper part of OB-I defines the Anorthosite subzone and is primarily composed of anorthosite, leucotroctolite, and norite (Todd et al. 1982).

Above OB-I, rocks return to their mineral sequences as seen in N-I and GN-I, forming GN-II and N-II, with pronounced modal layering again becoming common just below OB-II. Mineral compositions in GN-II and N-II are otherwise more evolved than in the lower units (McCallum et al. 1980; Todd et al. 1982; Barnes and Naldrett 1986; Jenkins et al. 2021). Indeed, mineral composition trends from below to above OB-I continue nominally monotonic fractionation trends with little evidence of compositional offsets. This is most evident in the core compositions of plagioclase (Fig. 1b), which is both the most persistent mineral through

OB-I and is resistant to trapped liquid shift effects. Pyroxene Mg# is more variable up through the section (perhaps reflecting variable trapped liquid re-equilibration), but overall, the pyroxenes show similar fractionation effects (e.g., decreasing Cr concentrations upward) as well.

While major mineral compositional trends show a continuous fractionation trend throughout the Lower Banded series, OB-I does mark a distinct change in the Cl/(Cl + F) ratio in apatite. Apatite below OB-I is predominantly chlorapatite in composition but trends to more F-rich compositions within and above OB-I (Boudreau and McCallum 1989). Where affected by later alteration/serpentinization the chlorapatite can be altered, in part, to hydroxyapatite (Boudreau and McCallum, 1990).

Previous interpretations of OB-I and the J-M reef

Models for the petrogenesis of OB-I and the J-M Reef range from strictly orthomagmatic to those that involve volatile fluids and flux melting. Several models are discussed here, with an emphasis on the hydration melting model.

Early models were largely orthomagmatic but involved a variety of crystallization scenarios. Irvine et al. (1983) proposed a mechanism involving olivine saturation during mixing of magmas of Ultramafic series affinities ("U-type" magma that crystallized much of the underlying rocks) with an anorthositic magma affinity typical of the Middle Banded series ("A-type" magma responsible for crystallization of anorthosites) in a double-diffusive convective mixing model. Noting that the high PGE tenors of sulfide require high magma/sulfide mass ratios, Barnes and Naldrett (1986) suggested that pulse of magma is credited to have entered the Stillwater chamber as a buoyant plume that spread out to form a layer of hybrid liquid layer high in the chamber. Sulfide liquids are thought to obtain high PGE concentrations due to turbulent ascent up the plume and settling though a thick layer of magma. Olivine is crystallized and pre-existing plagioclase undergoes melting within the hybrid layer. These olivine-plagioclase-sulfide glomerocrystic "boulders" settle to the floor to produce the varitextured and heterolithic rocks characteristic of the reef.

More recently, Keays et al. (2012) takes a totally orthomagmatic approach in which the J-M Reef is interpreted to have formed from a magma that was enriched in the PGE owing to interactions with S-bearing crustal rocks. This S- and metal-rich magma is then re-dissolved in a smaller volume of magma before it enters the main Stillwater chamber to form the J-M Reef. Godel and Barnes (2008) suggested a similar two-staged approach to reef formation, one that involves a magmatic constituent that brings in the initial PGE, Ni, Cu, and Te contained in a magmatic sulfide liquid, followed by possible sulfur loss and secondary upgrading by a Pd-rich, S-poor fluid. Following on this study, Barnes et al. (2020) suggested a process involving the partial melting of a komatiitic massive sulfide at depth and transport of metal-enriched sulfide droplets. Ripley et al. (2017) suggested that sulfur from country rock was involved in the formation of the J-M Reef. They similarly suggest immiscible sulfide liquid becoming enriched in staging chambers to the Stillwater Complex. Their S isotopic data is otherwise indifferent as to support for a magmatic sulfide collection model or fluid transport model.

Boudreau (1988, 1999a, 2016) highlighted the lack of compositional offsets expected by a new influx more primitive magma, the relative abundance of hydrous minerals in the more olivine-rich rocks, the change from Cl-rich apatite to more F-rich apatite across OB-I, the hydrous inclusions in chromite and other phases interpreted as crystallized from hydrous liquids, the Cl-rich nature of fluid inclusions found in pegmatoids below the J-M Reef and their local enrichment in the PGE-sulfide, the rounded and reversely-zone plagioclase and the pegmatitic textures characteristic of the more olivine-rich rocks of OB-I and the formation of apophyses of olivine-rich rocks into overlying layers. He suggested that olivine was the result of incongruent melting as ore-bearing fluids percolated upward into hotter rocks that were not yet vapor saturated. In brief, the addition of H_2O has the following effects: Olivine is stabilized at the expense of pyroxene, phase diagram isotherms will migrate in a way in which at any given temperature, the amount of liquid will increase with the addition of H_2O, spinel stability is enhanced (e.g., Ford et al. 1972; Mathez and Kinzler 2017; Veksler and Hou 2020), plagioclase stability relative to mafic minerals is depressed (e.g. Holloway and Burnham 1972; Helz 1976; Rutherford et al. 1985), and finally high volatile contents can lower viscosity, increase diffusion and promote mineral growth. The hydration melting model is analogous to models for arc magmatism where volatiles coming off a subducting slab cause partial melting in the overlying hotter mantle wedge. The presence of PGE-rich, massive sulfide cores to some pegmatoids was considered as strong evidence that the ore components can be readily mobilized by late fluids.

Accepting the evidence for the presence of fluids presented by Boudreau but rejecting it as the source for the ore component of the J-M Reef, Barnes and Campbell (1988) suggested that fluids were only a secondary overprint to a primarily magmatic process. Their model argues that the presence of hydrothermal features is a result of a lower solidus temperature of the olivine orthocumulates that can trap fluids migrating upward through the crystal pile. Except for the additional crystallization of hydrous minerals and the development of coarser textures, the fluids are otherwise unrelated to mineralization and the reappearance of olivine.

Jenkins et al. (2021) accepted evidence that olivine was the result of incongruent melting but suggested this was driven by the downward percolation of a superheated magma and not the result of hydration. They modeled the mineral assemblages in OB-I by partial remelting of the gabbronorite and norite cumulates by the influx of an what was initially a contaminated komatiitic liquid that was undergoing parallel fractionation in the lower crust. They show using MELTS modeling that the olivine bearing rocks could form by the reaction of this hot magma with mushy gabbronoritic floor rocks. They also suggested that Reef formation involved reaction with sulfide-saturated floor rocks with the incoming magma.

Methods

In this paper, a more detailed modeling of volatile influence on crystallization is undertaken than was done earlier (Boudreau 1988, 1999a; Boudreau and McCallum 1989). In this study, the MELTS and PELE programs were used to model hydration melting of norite, gabbronorite and melanorite bulk compositions. Modeled mineral compositions and modal abundances, including sulfide, are compared with those of OB-I and the J-M Reef.

MELTS modeling

The thermodynamic modeling program MELTS for Excel (Gualda and Ghiorso 2015, rhyolite-melts version 2) was used to add mixtures of H_2O or $Na_2O + H_2O$ to a range of Stillwater protoliths, whose compositions were averaged from bulk rock samples published in Jenkins et al. (2021) from a single drill core representing the stratigraphy of the Lower Banded series in and below OB-I. The exception is a melanorite composition reported by Barnes et al. (2020, sample ST-05). A small amount of H_2O (0.01 wt.%) was added to each bulk composition to stabilize possible hydrous minerals (e.g., apatite) in the initial "dry" mineral assemblage. Because Cr is not accounted for in MELTS pyroxene solid solution models, it was not included in the bulk averages. The averaged bulk compositions and calculated CIPW norms for the norite, gabbronorite and melanorite protoliths used for modeling, along with average composition of troctolite and the more olivine-rich peridotite/harzburgite rocks of OB-I, are listed in Table 1. Average trace element abundances are listed in Table 2.

Modeled batch equilibrium melting of the bulk compositions as a function of temperature at pressure 2 kbar for the nominally "dry" protoliths with oxygen fugacity constrained to the QFM oxygen buffer are shown in Fig. 3. For all bulk compositions, 1050 °C was well-below the initial mush temperature of 1150–1175 °C suggested by Jenkins et al. (2021) and was used as the hydration temperature. Simple heating of the protolith above their initial crystallization temperature does not produce olivine by incongruent melting. However, a small amount of relatively Mn-enrich olivine is present in the model near-solidus assemblages that is not observed in the rocks. This is likely due to components (such as Cr noted above as well as Mn) not accounted for in the MELTS mineral solid solution models. The initial model modes and mineral compositions are otherwise similar to those reported by Jenkins et al. and the discrepancy can be considered a

Table 2 Representative average trace element compositions of rocks from Olivine-Bearing zone I of the Stillwater Complex

	1	2	3	4	5
	Norite	Gabbronorite	Melanorite	Troctolite	Peridotite
Sc (ppm)	16	28	26	7	17
V	68	99	128	31	69
Cr	343	1540	1460	40	1651
Co	29	33	74	40	126
Ni	190	243	528	423	1389
Cu	40	20	26	108	62
Zn	40	35	48	40	67
Ga	12	9	6	12	3
Ge	1	1	-	1	1
Rb	1	1	1.6	< 1.0	2
Sr	107	66	33	112	22
Y	2.6	3.4	2.8	1.8	2.7
Zr	7	9	6	6	12
Nb	1.7	7.3	0.28	1.6	0.4
Ba	27	15	16	26	8
La	0.83	0.79	0.88	0.87	0.63
Ce	1.50	1.53	1.66	1.54	1.24
Pr	0.18	0.21	0.21	0.19	0.17
Nd	0.82	0.90	0.85	0.81	0.76
Sm	0.23	0.29	0.2	0.20	0.24
Eu	0.217	0.145	0.12	0.210	0.086
Gd	0.31	0.41	0.27	0.27	0.34
Tb	0.06	0.08	0.05	0.05	0.07
Dy	0.42	0.54	0.43	0.30	0.45
Ho	0.09	0.12	0.1	0.06	0.10
Er	0.28	0.36	0.33	0.18	0.30
Tm	0.045	0.057	0.06	0.028	0.048
Yb	0.32	0.41	0.07	0.19	0.33
Lu	0.051	0.064	0.4	0.030	0.052
Hf	0.1	0.2	0.2	0.1	0.3
Ta	0.40	1.51	0.04	0.31	0.11
Tl	< 0.05	< 0.05	0.02	< 0.05	0.1
Th	0.08	0.18	0.17	0.07	0.28
U	0.03	0.11	0.06	0.02	0.05

Notes 1. Melanorite from Barnes et al. (2020), all others from Jenkins et al. (2021), average of several samples each as for Table 1

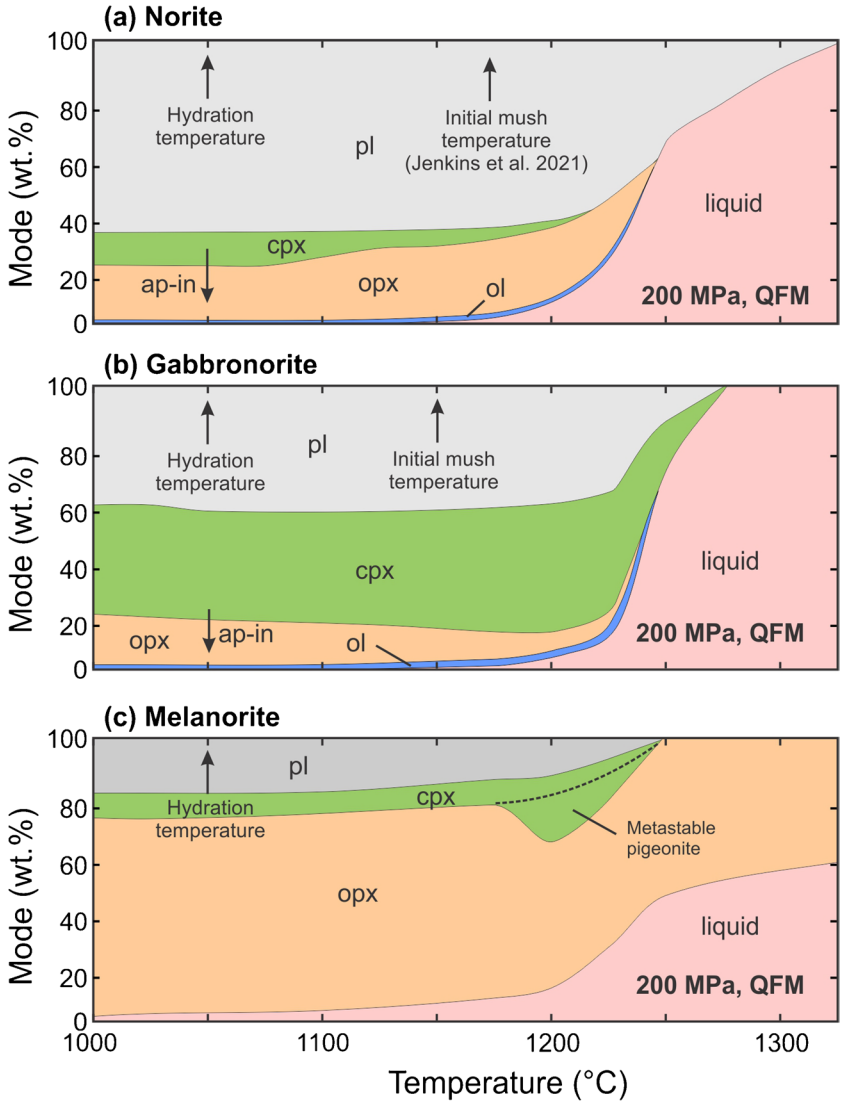

Fig. 3 Batch (closed system except for O_2) melting behavior of the **a** norite, **b** gabbronorite and **c** melanorite protoliths listed in Table 1 as a function of temperature at 200 MPa pressure, and $f(O_2)$ constrained to the QFM buffer. Estimates of the initial mush temperature for the norite and gabbronorite noted on the graphs are from Jenkins et al. (2021). A hydration temperature of 1050 °C, also marked, was used for the hydration modeling in this study. Note metastable pigeonite that occurs in melting of the melanorite. Abbreviations used here and subsequent figures: cpx, clinopyroxene; opx, orthopyroxene; ol, olivine; pl, plagioclase; ap, apatite; bt, biotite; sp, spinel

measure of the uncertainty of the model results. The free energy minimization algorithm can occasionally produce metastable results (as seen in the presence of pigeonite in Fig. 3c), particularly when a phase is near saturation. These spurious results can disappear with modest changes to crystallization conditions (T or $f(O_2)$, for example). Standard practice is to include pigeonite along with the other low-Ca pyroxene orthopyroxene or to interpolate between stable steps.

Although MELTS includes CO_2 as a possible gas species, hydration melting was initially modeled by adding a pure H_2O fluid as CO_2 mainly limits H_2O solubility and its fluxing effects (but see PELE modeling below). However, Stillwater fluid inclusions are composed of variable amounts of dissolved components and especially the alkalis NaCl and KCl (Hanley et al. 2008). To model the effect of a more natural, alkali-rich fluid, a 50 wt.% H_2O + 50% wt.% Na_2O "faux brine" was used to model halide-rich fluid addition. This is justified by the observation that Cl is about twice the molar weight of O and that it takes two moles of univalent Cl^- anion to substitute for one mole of the divalent $O^=$ anion, or about 0.25 wt.% O_2 are replaced by every 1.0 wt.% Cl added. Given that the total fluid mass added in the MELTS runs is not more than 5 wt. % and as Cl would be distributed among all anion sites in the silicate liquid and not just Na^+, it is assumed that addition of NaCl can be approximated by the addition of Na_2O alone. This does demonstrate the need to expand the MELTS model to incorporate more non-standard components.

Pele modeling

Modeling with PELE v8.01 (Boudreau 1999b) was used to constrain the effects of both an H_2O-rich and a CO_2-rich fluid as mineralizing agents. PELE includes a more complete C-O–H-S fluid composition, allows for immiscible

sulfide saturation in the silicate liquid, and includes Cl and F as a silicate liquid components. The phase equilibration engine in PELE is used in the reaction-mass transfer program IRIDIUM, the latter of which has been used to model the formation of the chromitite-sulfide seams that occur at the top and bottom of the Merensky Reef pegmatoid of the Bushveld Complex (Boudreau 2008). The PELE/IRIDIUM source code is available as part of the on-line supplemental material.

The composition of the H_2O-rich and CO_2-rich fluids added to the protolith are taken to be representative of a natural solution, with other components estimated either from the fluid inclusion compositional ranges reported by Hanley et al. (2005) (e.g., Fe, Al, Na, K, Cl), estimates of fluid solubilities (e.g., Si) or by requirement that the fluid itself not initially be sulfide saturated (e.g., S). Ore metal concentrations for Ni, Cu, Pd and Pt of the fluid are constrained by the need to reproduce the ore grades of the J-M Reef. Because hydration melting of the melanorite produced a peridotite assemblage that most closely resembled the olivine-rich rocks that most commonly host the J-M Reef, these fluids were added to the melanorite under the same conditions as for the MELTS runs. The compositions of the two fluids and partition coefficients used in the modeling are listed in Table 3. Also shown for comparison are the ranges reported for Stillwater fluid inclusions by Hanley et al. (2005, 2008). Run results are shown in the spreadsheets in the supplemental material, where one can change initial ore metal concentrations in the fluid as well as partition coefficients to investigate conditions not covered in this report.

Results

MELTS modeling: pure H_2O fluid

The change in phase proportions of the norite, gabbronorite, and the melanorite protoliths as a function of the mass of pure H_2O added is shown in Fig. 4. Hydration resulted in increased silicate liquid and crystallization of olivine at the expense of orthopyroxene, with clinopyroxene changing very little, presumably being stabilized by the release of Ca from the melting of plagioclase. The maximum olivine produced in the norite was 11.0 wt. % at 1.5 wt. % H_2O added, 9.9 wt. % olivine at 1.5 wt. % H_2O for the gabbronorite, and 26.8 wt. % olivine at 3.0 wt.% H_2O for the melanorite, decreasing slowly with additional fluid added. Melting stopped once each system became saturated in pure H_2O vapor between ~ 2–3 wt.% added H_2O as shown in Fig. 4. Figure 5a shows the variation in the Fo content of

Table 3 Parameters for PELE model of hydration of Melanorite Protolith

	Melanorite Protolith	Brine inclusions[1]	H_2O-rich fluid	CO_2-rich fluid		
SiO_2 (wt.%)	53.80	-	1.13	1.10		
TiO_2	0.14	-	0.00	0.00	Partition coefficients	
Al_2O_3	8.47	0.02—0.19	0.00	0.00	D(sulfide/Liquid)	
FeO(total)	8.50	2.44—8.36	0.57	2.00	Pt	80,000
MnO	1.18	1.42—4.65	0.00	0.00	Pd	80,000
MgO	21.80	0.02—0.17	0.00	0.00	Ni	800
CaO	6.62	4.76—15.1	5.71	5.62	Cu	1,200
Na2O	0.42	14.7—28.6	25.2	5.91		
K2O	0.04	2.16—4.92	5.71	5.60	D(vapor/liquid)	
P2O5	0.02	-	24.0	5.91	Pt	10
H2O	0.01	-		1.13	1.02	Pd 10
CO2	0.00	-		0.00	0.00	Ni 10
S	0.01	-		39.2	9.91	Cu 10
F	0.001	-		6.43	66.7	
Cl	0.02	17.3–48.8	24.0	4.92	D(olivine/liquid)	
O = F, Cl, S	0.00	-3.90—-11.0	-9.47	-2.16	Ni	10
sum	100.0	38.9—99.7	100.0	100.0		
Pt (ppm)	0.1	0.4—4.0	100	25		
Pd	0.1	0.4—4.0	250	75		
Ni	400.0	100—1000	20,000	2000		
Cu	100.0	100—1000	5000	250		

Notes: 1. Range in brine inclusions reported by Hanley et al (2005, 2008) shown for reference. Element wt. % converted to oxide equivalents: low totals reflect variable H_2O-CO_2-CH_4

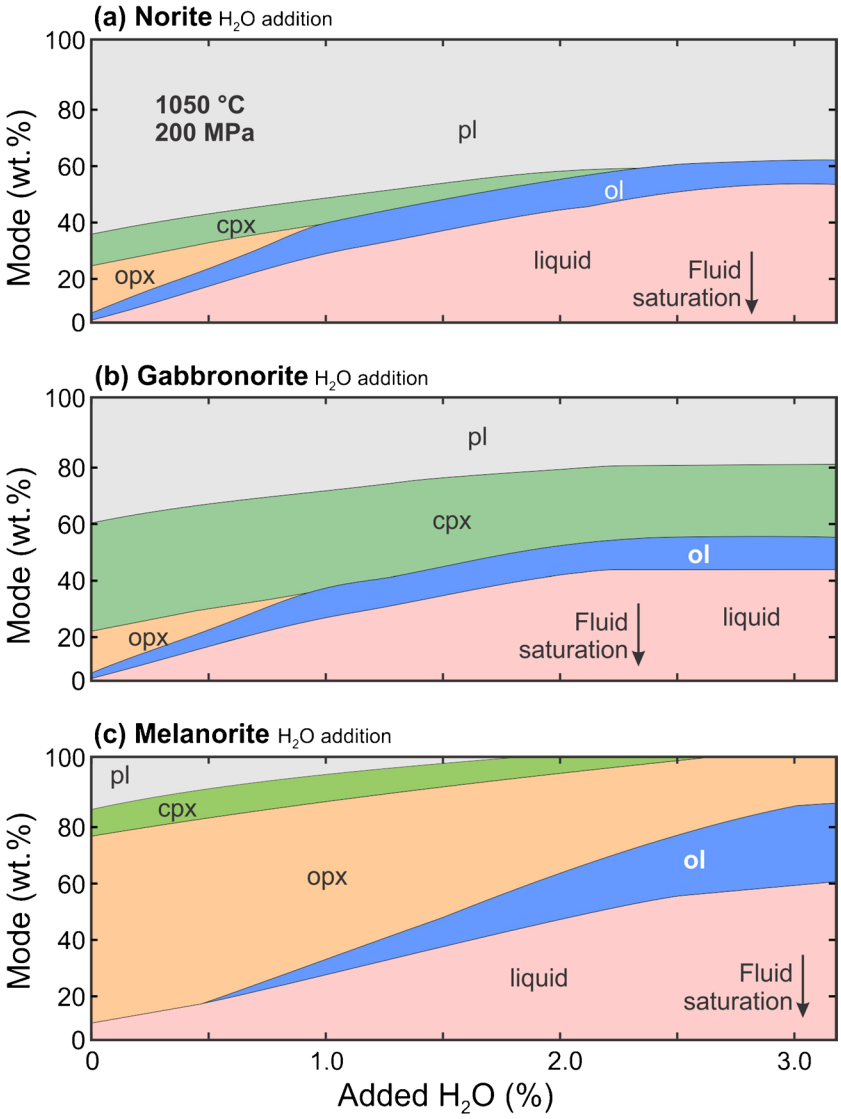

Fig. 4 MELTS results for the hydration melting with stepwise addition of pure H_2O fluid to the three protoliths **a** norite, **b** gabbronorite and **c** melanorite at 1050 °C, 0.2 GPa, and $f(O_2)$ = QFM. Labeled arrows on each plot show the point where each system became saturated in a pure H_2O fluid. Abbreviations as for Fig. 3

olivine as a function of the isothermal addition of H_2O, the olivine becoming modestly more magnesian with increasing melting. The maximum, Fo_{86}, occurs in the hydrated gabbronorite, otherwise olivine compositions for the other protoliths fall within the observed range of olivine (73–85) reported in Jenkins et al. (2021). (The sharp drop to lower Fo values near the start of hydration represents the Mn-enrichment in the small olivine nominally present in the "dry" bulk composition and not accommodated in other phases such as spinel noted above.)

Mineral compositions will re-equilibrate on cooling, particularly with reaction with any retained interstitial liquid. With no loss of the hydration melt, the olivine will completely react to form the original amount of pyroxene (± amphibole, the amount depending on the amount of water lost to degassing or diffusion away from the hydrated rocks), whereas the complete loss of the hydration melt liquid at the hydration temperature would preserve the phase assemblages that were produced by the 1050 °C melting event. The preservation of some of the hydration melt in the cooling assemblage will fall somewhere in between. To split the difference, half of the liquid mass produced at the H_2O amount that resulted in the maximum olivine produced was removed from all three partly molten assemblages and these new bulk compositions cooled from the initial hydration temperature of 1050 °C down to 850 °C as a closed system (Fig. 5b). For example, if the maximum olivine produced occurred at 2 wt. % H_2O added and for which the hydrated assemblage produced 30% liquid, then a new bulk composition was constructed using the model mineral compositions and their masses but using only half the mass of the hydration melt (15 wt. %).

Examples of post-hydration changes during cooling after loss of 50% of the hydration melt are shown in Figs. 5b and c. Although olivine typically becomes modestly more Fe-rich on cooling (Fig. 5b), the modeled

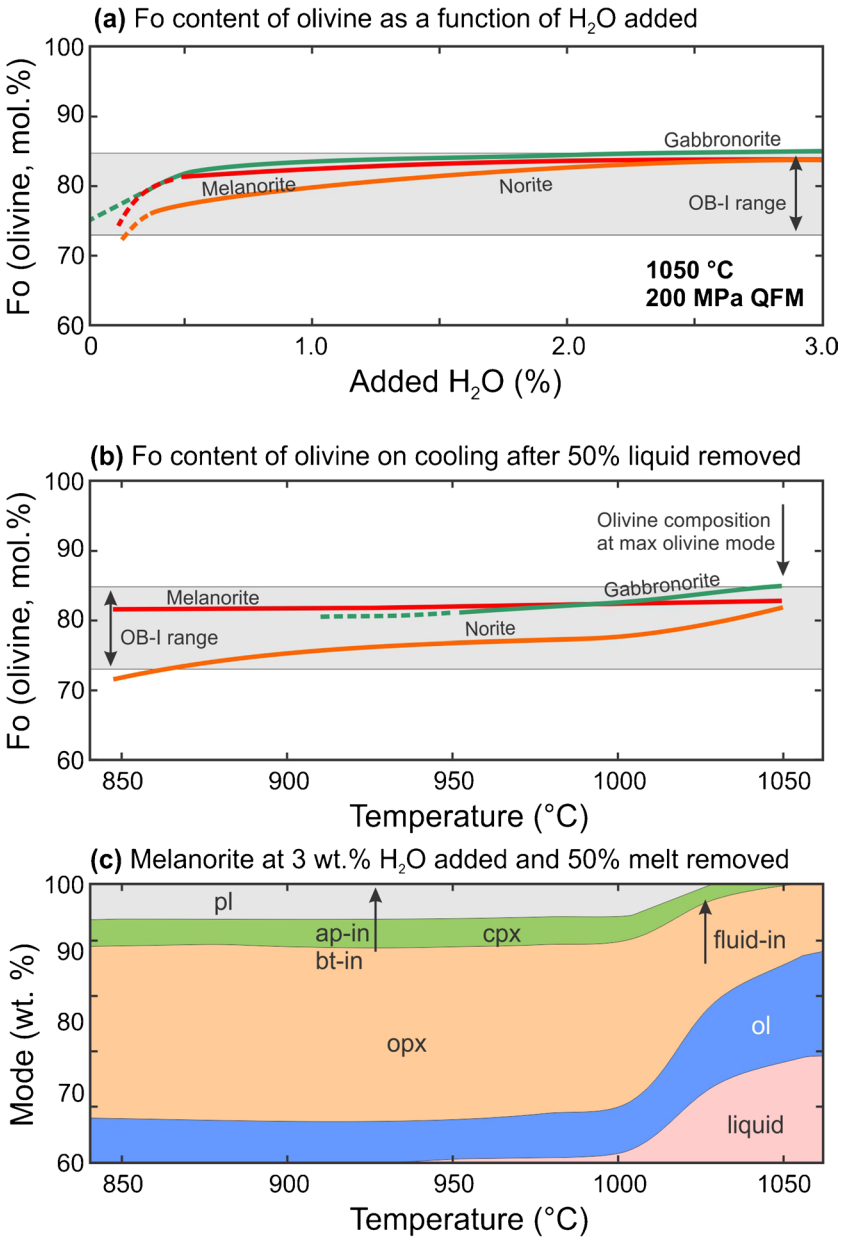

Fig. 5 **a** MELTS results showing variation of the Fo content of olivine as a function of pure H_2O fluid added to the three protoliths at 1050 °C. **b** MELTS results showing variation of the Fo content of olivine as a function temperature for the three assemblages after loss of half of the generated hydration melt at the added H_2O that produced the most olivine at 1050 °C. Grey shaded areas are range of OB-I olivine compositions reported by Jenkins et al. (2021). c) Example of the modal changes on cooling of the melanorite after 3.0 wt.% H_2O added at 1050 °C and half the resultant melt removed prior to cooling. Modal changes on cooling for the other starting compositions are shown in supplemental figure S1. The various phase "-in" points are temperatures at which these phases occur on cooling. All results calculated at 0.2 GPa and $f(O_2)$ = QFM. Abbreviations as for Fig. 3

olivine Fo content continues to overlap with the ranges observed in OB-I, with most of this equilibration occurring in the first 50 °C. The gabbronorite did not produce stable results below about 950 °C. Modal changes for the most olivine-rich assemblage produced by the hydration melting of the melanorite as shown in Fig. 5c (result for the other runs are shown in supplemental material Figure S1). Solidification of the residual liquid and peritectic reaction of olivine with the residual liquid results in the replacement of about half of the olivine by orthopyroxene, again mostly occurring over the first 50 °C where most of the liquid solidifies. This loss of olivine to peritectic reactions with residual liquid occurs for the other initial starting compositions as well.

Plagioclase and hydrous mineral variations are discussed along with the faux brine results separately below.

MELTS modeling: faux brine fluid

Phase proportions as a function of the mass of 50% H_2O + 50% Na_2O faux brine added to the three protoliths are shown in Fig. 6. Owing to the addition of another fluxing component, Na_2O, in addition to H_2O, more fluid can be added before the system saturates in a pure H_2O fluid; none of the runs became fluid-saturated at 5 wt.% faux brine added. The main difference from the pure H_2O fluxing runs is that olivine itself can melt and disappear as flux melting advances. The maximum olivine production varied

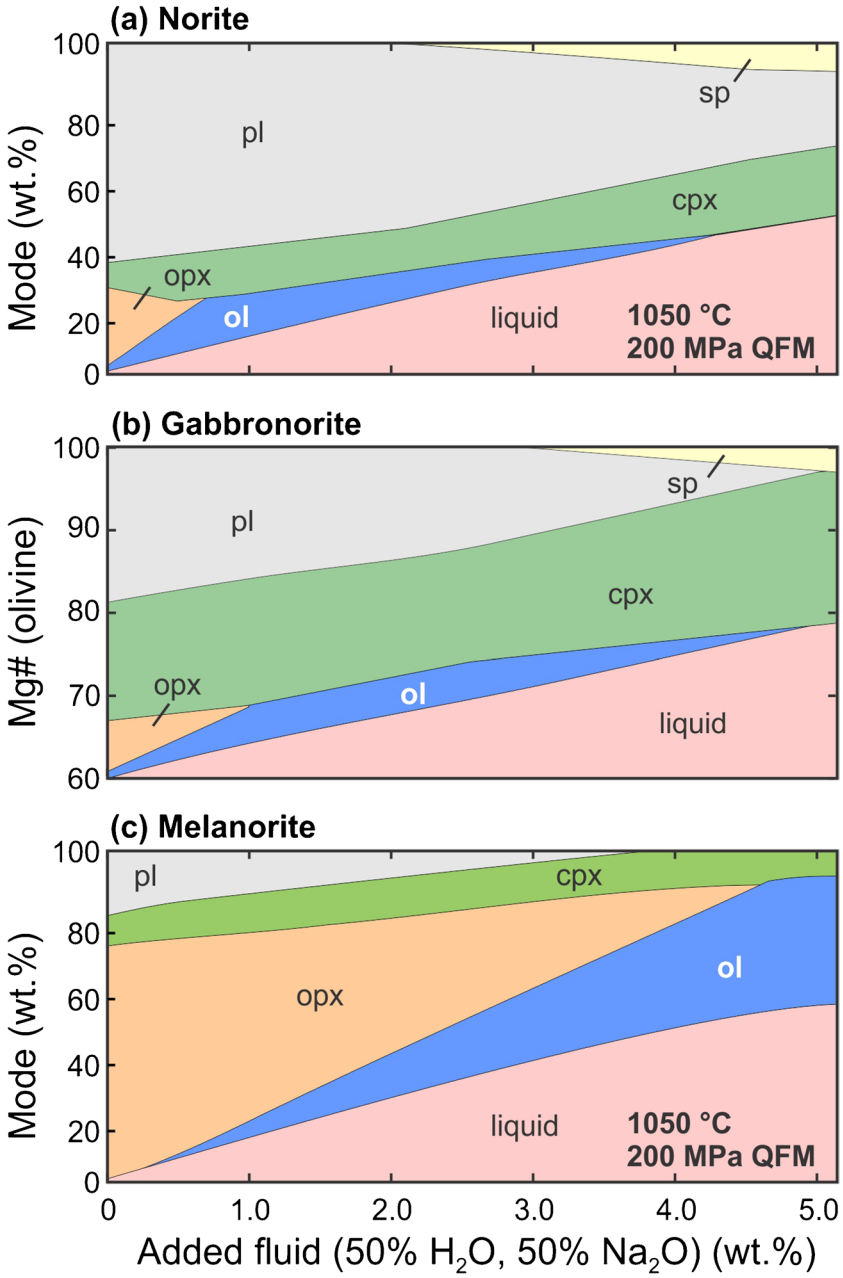

Fig. 6 Fig. 4. MELTS results for the hydration melting with addition of 50% H_2O + 50% Na2O "faux brine" fluid to the three protoliths **A** norite, **B** gabbronorite and **C** melanorite at 1050 °C, 0.2 GPa, and $f(O_2)$ = QFM. Note that olivine reaches a maximum modal abundance for the norite and gabbronorite protoliths before it melts out at higher fluid mass added. Abbreviations as for Fig. 3

depending on the protolith, occurring at 5 wt. % added fluid for the melanorite, 1.5 wt.% fluid for the gabbronorite and at 1 wt. % fluid for the norite. Again, the maximum amount of olivine produced is a function of the amount of orthopyroxene in the original protolith. The final composition of the melanorite was essentially composed of olivine (37 wt.%) and silicate liquid and lesser amounts of clinopyroxene.

Changes in olivine composition as a function of both isothermal fluid addition and cooling are shown in Fig. 7. As for the pure H_2O addition runs, all compositions produce a more Mg-rich olivine as melting advances, the highest again occurring in the hydrated gabbronorite (Fo_{87}, Fig. 7a). Olivine compositional changes on cooling were again modeled using the hydrated assemblages at the fluid added amount that produced the maximum amount of olivine, but again with half of the partial melt produced at 1050 °C removed. Cooling of these modified bulk compositions resulted in the partial replacement of olivine with orthopyroxene and lowering the Fo content of the olivine. The re-equilibrated olivine compositions fall within the range of observed OB-I olivine (Fig. 7b). As for the H_2O-only runs, olivine produced by the hydration is partially lost by peritectic reaction with the residual liquid on cooling (Fig. 7c and supplemental figure S1).

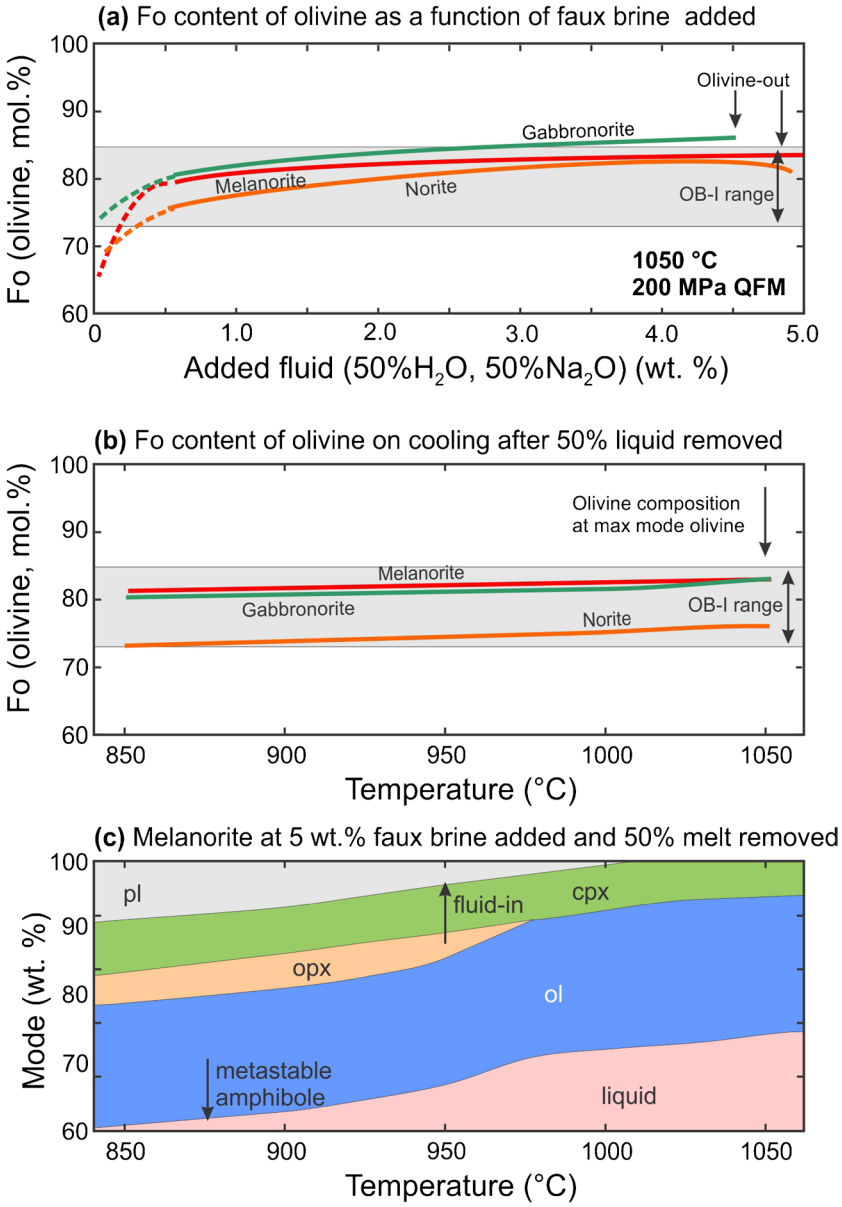

Fig. 7 **a** MELTS results showing variation of the Fo content of olivine as a function of the mass of the 50% H_2O + 50% Na_2O "faux brine" fluid added to the three protoliths at 1050 °C, **b** MELTS results showing variation of the Fo content of olivine as a function temperature for the three assemblages at the maximum modal olivine produced during hydration at 1050 °C as shown in Fig. 6 and after loss of half of the generated hydration liquid. For both, the grey shaded areas are range of olivine composition from OB-I reported by Jenkins et al. (2021). **c** Example of modal changes during cooling of the melanorite after loss of half the melt produced by addition of 5 wt.% faux brine at 1050 °C. "Fluid-in" denotes fluid saturation temperature on cooling. Modal changes on cooling for the other starting compositions are shown in supplemental figure S1. All results were calculated at 0.2 GPa, and $f(O_2)$ = QFM. Abbreviations as for Fig. 3

MELTS modeling: plagioclase and minor phases

Variations in plagioclase AN concentrations are shown in Fig. 8 for both the pure H_2O fluid and the faux brine runs. The plagioclase compositions of the initial protoliths all fall in the middle of compositional range for "cumulus" primocrysts reported by Jenkins et al. (2021). For the pure H_2O runs, the plagioclase trends to a sharp increase towards higher AN composition for all protoliths with added H_2O, to a maximum of ~ AN_{92} (Fig. 8a). For the faux brine runs (Fig. 8b), this increase in the AN component is moderated for the hydrated norite and gabbronorite compositions, as would be expected by the addition of Na_2O into the system by the fluid. For the melanorite faux brine case, the minor plagioclase content of the original protolith is overwhelmed by the added Na_2O such that the equilibrium plagioclase becomes more albitic as hydration melting advances until plagioclase melts out at ~ 3.5 wt.% faux brine added.

Comparison of model results with observed plagioclase compositions from OB-I is problematic owing to the resistance of plagioclase to solid-state re-equilibration and which instead tends to develop compositional zoning. It is further complicated by continuous melting of the plagioclase that can destroy the modified rims as fast as they re-equilibrate. Nonetheless, where primocrysts of plagioclase are present in the olivine-bearing assemblages, it tends to be modestly reversely zoned (Fig. 8c, Barnes and Naldrett 1986). The magnitude of this reversal is similar to that seen in the faux brine runs and much smaller than expected from the pure H_2O runs. Otherwise, the plagioclase compositions

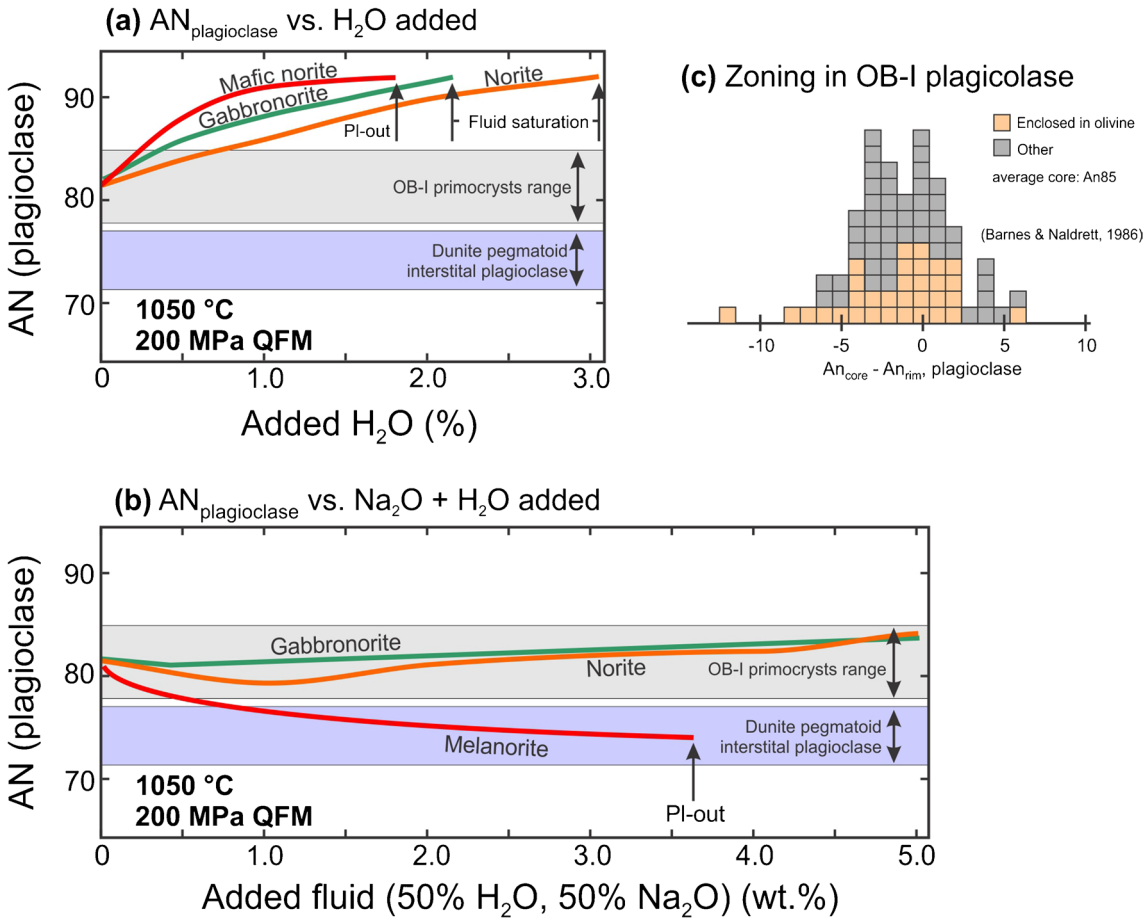

Fig. 8 Variation in the composition of plagioclase as a function of **a** pure H_2O fluid added and **b** 50% H_2O + 50% Na_2O "faux brine" added to the three protoliths at 1050 °C, 0.2 GPa, and $f(O_2)$ = QFM. Grey shaded areas are range of plagioclase core composition of plagioclase primocrysts from norites, troctolites and gabbronorites from OB-I and the blue shaded areas are the range of interstitial plagioclase from rocks described as pegmatoidal dunites, both from data of Jenkins et al. (2021). **C** A plot of $AN_{core} - AN_{rim}$ compositions from OB-I (data from Barnes and Naldrett 1986). Abbreviations as for Fig. 3

for the norite and gabbronorite faux brine runs tend to fall within the range of OB-I "cumulus" plagioclase reported by Jenkins et al. (2021) whereas the pure H_2O runs rapidly move out of this range with added H_2O. The plagioclase from the melanorite runs trend to the more albitic plagioclase compositional range reported by Jenkins for "intercumulus" plagioclase from what they describe as pegmatoidal dunites. They also approach the composition of plagioclase seen in gabbroic pegmatoids beneath the reef (Fig. 1b and Braun et al. 1994).

Apatite was the only hydrous mineral stable in the original protoliths and that reappears crystallization of the hydration melts. Amphibole and biotite begin to appear below ~ 950 °C, typically as metastable minerals that come and go and were more likely to appear in the faux brine runs than the pure H_2O runs presumably owing to lower solidus temperatures. For example, 37% amphibole appeared at 875 °C for cooling of the hydrated norite (with half the hydrated melt removed as described previously) where it completely replaces the pyroxene, but it is absent when equilibrated at 850 °C. Modeling a faux brine that also included K_2O as well as Na_2O could stabilize more biotite. However, given that the interstitial liquid becomes fluid-saturated on cooling and that this exsolved fluid could be lost prior to amphibole/biotite stability, these results are only suggestive of the upper temperature stability limits for these minerals.

PELE modeling results

As noted above, the PELE modeling was mainly to look at sulfide precipitation and a more realistic C-O–H-S-X fluid. Because mineralization is most commonly described as being associated with the more olivine-rich rocks, only results using the melanorite protolith composition are shown. This composition also requires the most added Ni

to account for Ni content of olivine as well as the sulfide, thus requires the highest fluid Ni concentration. Results are otherwise broadly similar for other protoliths.

Results for the addition of the H_2O-rich solution and the CO_2-rich solution are shown in Fig. 9, where for each run the results are plotted in four graphs against fluid added for 1) silicate mineral modes (wt.%), 2) immiscible sulfide liquid and fluid modes (wt.%), 3) the $\log_{10}$ concentration of the four ore metals in the sulfide fraction, and 4) the nominal $\log_{10}$ ore grade of the four metals, calculated as equal to the metal concentration in sulfide x wt. fraction sulfide (Ni includes olivine in this calculation). For the latter two pairs of plots, average J-M Reef values are shown as the heavy dashed lines.

For the H_2O-rich fluid run, hydration melting of the protolith is similar to the MELTS runs, producing an olivine-bearing assemblage, but unlike the MELTS runs clinopyroxene also melts out. The assemblage also becomes fluid-saturated at about the same point at just over 3% H_2O added. The added fluid leads to saturation in an immiscible sulfide early, and even after the system is fluid saturated sulfide continues to precipitate as the fluid continues to add sulfur to the system, to a maximum modal abundance of just over 0.5 wt.%. However, above about 5 wt.% fluid added,

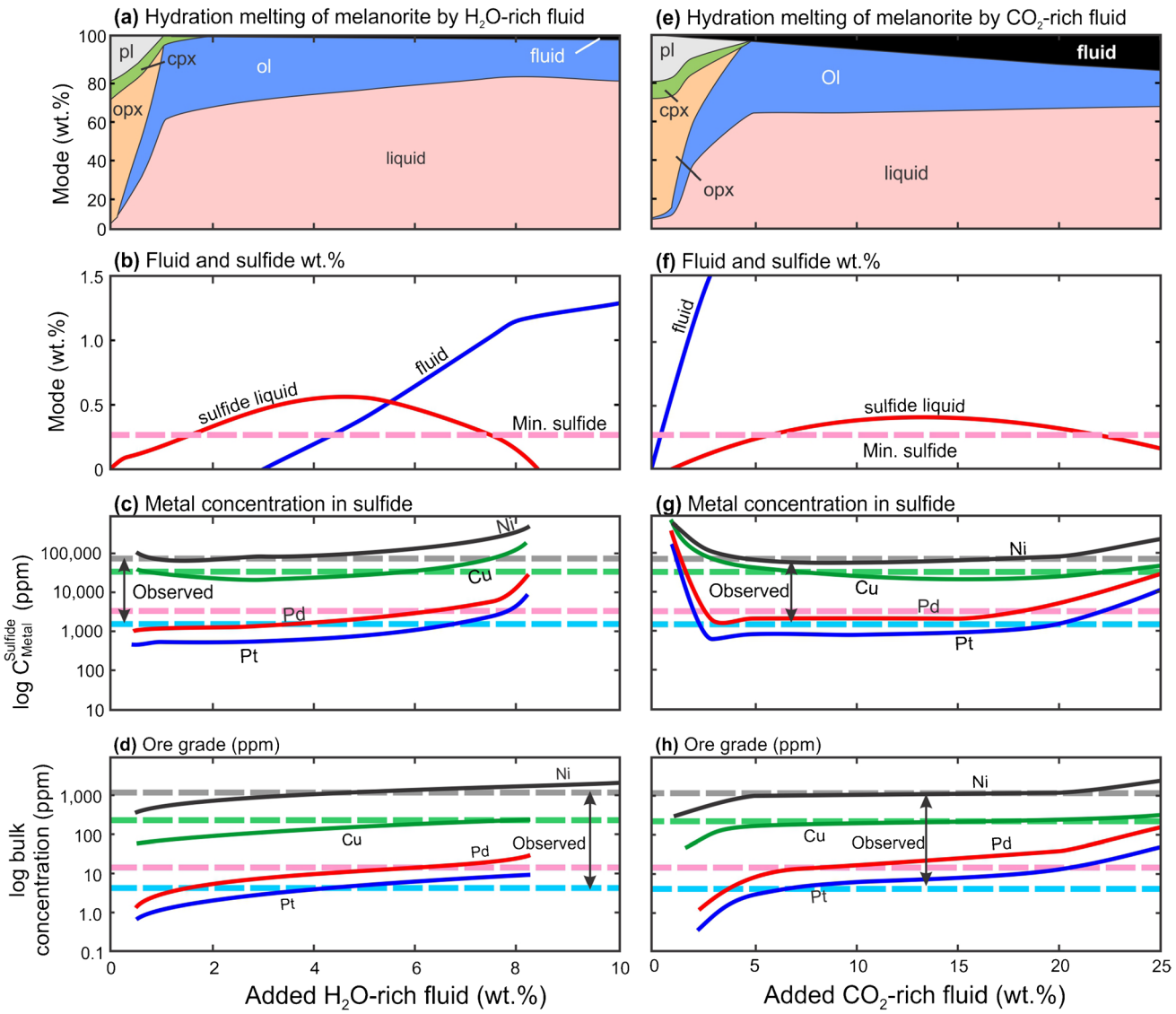

Fig. 9 Results of PELE modeling for hydration of the melanorite protolith for both an H_2O-rich fluid (plots a-d) and a CO_2-rich fluid (plots e–h) at 1050 °C, 0.2 GPa and $f(O_2)$ = QFM. For each column of plots are shown the phase assemblage (**a** and **e**), the modal amounts of sulfide and fluid (**b** and **f**), the $\log_{10}$ concentrations of Cu, Ni, Pd and Pt in an immiscible sulfide liquid (**c** and **g**), and the $\log_{10}$ ore grade as describe in text (**d** and **h**), all as a function of total fluid mass added. Dashed lines show average values for the J-M Reef Stillwater River area (from Barnes and Naldrett 1985). Note also the higher total fluid mass added for the CO_2-rich fluid run. Abbreviations as for Fig. 3

sulfide is resorbed into the sulfide-undersaturated fluid until it is completely resorbed at just over 8 wt.% fluid added. Metal concentrations in the sulfide fraction and the ore grade generally increase with added fluid. As the sulfide is resorbed later in the reaction, the Pd and Pt concentrations increase modestly in the residual sulfide fraction owing to the strong partition preference of these metals for sulfide and because the metals are still being added by the fluid.

For the CO_2-rich fluid, the results are broadly similar, but the system becomes permanently saturated in fluid earlier, as expected for the higher concentration of the low solubility CO_2 component. Also, sulfide that is precipitated early is resorbed more slowly from its peak abundance of just under 0.5 wt.% at about 13 wt.% fluid. The sharp decrease in metal content of the sulfide just past the start of the hydration is due to all the metals going into a smaller sulfide fraction than for the H_2O-rich fluid.

Although not shown, apatite compositions vary from F-rich in the melanorite protolith prior to fluid addition to more Cl-rich compositions during the early stages of hydration before apatite is lost as melting advances with higher fluid addition. On cooling apatite can again reprecipitate as a chlorapatite, at which time it can trap samples of the observed alkali-rich hydrated melt inclusions found in apatite (Boudreau et al. 1986).

Added ore components to match the observed ore grades require fluid to contain 25-100 ppm Pt, 75–250 ppm Pd, 0.2–2.0 wt.% Ni, and 0.03–0.30 wt.% Cu, the higher values being required by the H_2O-rich model and the lower values for the CO_2-rich model. These values are constrained by the need for sulfide to be present; sulfide is lost early for the H_2O-rich fluid but is present at much higher fluid/rock mass ratios for the CO_2-rich fluid. The amount of sulfide precipitated is controlled by the S concentration of the original fluid, particularly for the CO_2-rich fluid. Variation of this parameter alone will change the sulfide tenors but not strongly affect the ore grade.

The results here are consistent with the discussion of sulfur and metal mobilization modeled by Boudreau and McCallum (1992) and Boudreau and Meurer (1999). Briefly, the PGE are rapidly depleted from the fluid as the early fluids add sulfur and induce sulfide saturation, given the high sulfide/melt partition coefficients (8×10^5) and modest vapor/liquid partition coefficients (10) used in the modeling (the spreadsheet in the supplemental material allows one to see the effect of changing various partition coefficients). As noted below, experimental values for vapor/liquid partition coefficients range from ~ 10–1,000. The preference for the PGE to partition into sulfide is thus at least 1–2 orders of magnitude higher than for any other phase. Furthermore, and unlike orthomagmatic models for which sulfide PGE tenor is critically dependent on variation in the partition coefficients and especially the R-ratio (the silicate liquid/sulfide liquid mass ratio (e.g., Campbell and Naldrett, 1979), PGE ratios for the hydrothermal model are largely a function of fluid composition. However, once sulfide is fully resorbed with additional fluid influx, the fluid becomes the next best host for the ore components for fluid/melt partition coefficients > 1. For the cases shown here, the fluid is not lost after it is added to the system to illustrate the mass of fluid involved. However, if mobile, it can result in late redistribution or loss of the ore components as discussed below.

Discussion

The MELTS modeling show that orthopyroxene is quick to melt out to produce olivine in all run conditions and all protoliths. Clinopyroxene melting is minor in the MELTS runs, it presumably being stabilized by the increase in Ca accompanying the melting of plagioclase, although this stability of clinopyroxene is not observed in the PELE runs. Olivine compositions mostly fall within the reported bounds of $Fo_{73–85}$ as reported by Jenkins et al. (2021) and within Barnes and Naldrett (1985) range of $Fo_{71–85}$, with the maximum Fo_{87} from the melting of the gabbronorite slightly higher than the observed range but which disappears with re-equilibration with residual liquid on cooling. The olivine continued to remain within the observed compositional bounds during cooling of the partially molten assemblages with half the melt removed, but with a modest Fe-enrichment in olivine as it re-equilibrates with the remaining liquid.

In no case was the Fo content of crystalized olivine as high as the Fo_{90} as modeled in Boudreau (1999a) and mentioned again in Jenkins et al. (2021) as a problem with the hydration model. However, the Boudreau study was done at 1250 °C (near-liquidus) as compared with 1050 °C for this study, nor did the earlier study look at later re-equilibration on cooling. To the degree that the hydration model is correct, and MELTS reproduces true mineral compositions, this would imply this current study is closer to the actual conditions.

Further support of the hydration melting model is shown by a comparison of the normative mineralogy of the modeled hydrated compositions with the olivine-bearing rocks of OB-I. Figure 10 shows the CIPW norm of both the hydrated norite and melanorite after loss of 50% of the flux melt for the faux brine runs as was done prior to cooling the new bulk compositions as shown in Fig. 7b. These are compared with the norms of an average troctolite and peridotite listed in Table 1. Although the choice of 50% melt loss was in part arbitrary, the normative minerals of both the modeled hydrated norite and melanorite are remarkably similar to the observed CIPW norm of an average troctolite and peridotite, respectively.

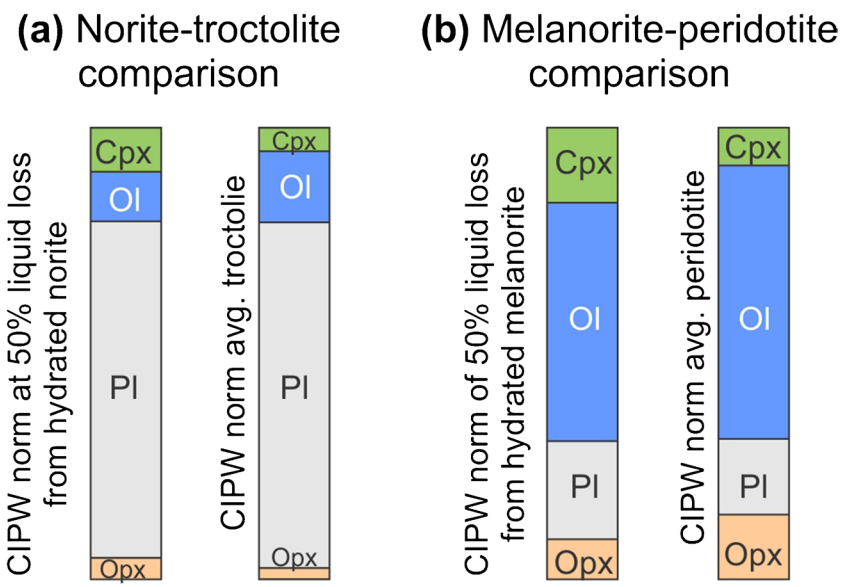

Fig. 10 Comparison of modeled and observed normative minerals for **a** the hydrated norite with 1.0 wt.% faux brine added and loss of 50% of the hydration melt vs. an average troctolite, **b** the hydrated melanorite with 5.0 wt.% faux brine added and loss of 50% of the hydration melt. vs. average peridotite. For each plot are shown the CIPW norm of the hydrated norite or melanorite after the loss of half of the hydration melt (left) and the average CIPW norm for the average troctolite or peridotite/harzburgite from OB-I listed in Table 1. Abbreviations as for Fig. 3

As noted earlier, the pegmatoidal peridotite such as shown in Fig. 2 can be interpreted as an olivine orthocumulte, a rock initially composted of "cumulus" olivine and a high proportion of intercumulus silicate liquid that underwent a peritectic reaction with the olivine on cooling (e.g., Barnes and Naldrett 1986). If this were the case, however, then one might expect the incompatible minor/trace elements such as P, Zr and U to be much higher than observed in the strongly "adcumulate" compositions of the norites and gabbronorites of OB-I. Instead, they are broadly similar (Table 2), as would be expected by hydration melting of a protolith already poor in incompatible elements.

The exception is Na. For the peridotites of OB-I that have only interstitial plagioclase, the conventional interpretation would suggest that the first interstitial plagioclase to crystallize would be expected to be within the range of "cumulus" plagioclase seen in the immediately surrounding rock, if not slightly more AN-rich. This is not observed; the interstitial plagioclase does not overlap but is distinctly more albitic than the primocrysts in the norite and gabbronorite (Fig. 8). That is, although the plagioclase that crystallizes from a residual liquid component will evolve to a more sodic plagioclase, one would expect the first cores to crystallize to be similar to that of the plagioclase crystallizing in the immediately surrounding rocks. Furthermore, and unlike mafic minerals, plagioclase does not readily re-equilibrate owing to slow solid-sate diffusion (plagioclase is commonly zoned). This re-equilibration is further expected to be limited owing to the coarser grain size of the interstitial plagioclase in the peridotites. This is why no one describes a "trapped liquid shift" effect for AN as is done for the mg# and instead note the size and nature of the compositional rims on plagioclase. This, the local abundance of interstitial biotite in the olivine-rich rocks, and the alkali-rich nature of the melt inclusions (e.g., Boudreau et al 1986; Boudreau 1988) are all consistent with the addition of alkalis by an alkali-rich fluid fluxing agent being the mechanism for troctolite/peridotite formation.

During closed system cooling, amphibole and biotite can become modally important minerals in the modeled compositions, particularly for the faux brine runs. Although these two minerals tend to be more common in the olivine-rich rocks than elsewhere other than pegmatoids (e.g., Boudreau 1988), it is nowhere near as abundant as the closed system models suggest. The natural and model systems need not be closed to loss of a volatile-rich melt and especially a vapor on cooling; loss of either would minimize hydrous silicate mineral crystallization. The exceptions are the aforementioned melt inclusions found in chromite and other phases, where the trapped liquid arguably crystallized as a closed system and the Na-amphibole and biotite are modally abundant, if not dominant.

Chromite is another sparse/minor mineral present in OB-I that was not modeled owing to the lack of Cr in the MELTS pyroxene solid solution models and hence no Cr_2O_3 was included in the protolith major element compositions of Table 1. If it were, the bulk Cr concentrations are high enough (especially in the gabbronorite) to saturate the system in a Cr-spinel, suggesting that chromite would saturate in the natural system as pyroxene is lost to melting during hydration. We note that the average bulk concentration of Cr in the gabbronorite and the peridotite of OB-I are similar (Table 2), consistent with the preservation of Cr by the early saturation in chromite during hydration. Otherwise the sparse nature of chromite may reflect peritectic reaction of the interstitial liquid and re-incorporation of Cr back into pyroxene.

Finally, although not modeled, the results suggest that modest hydration melting of a clinopyroxene-poor leuconorite can produce an anorthosite as the pyroxene and olivine both melt out with increasing flux melting. Loss of a significant fraction of the melt prior to cooling could result in a poikilitic pyroxene anorthosite.

Post-hydration effects

The modeling here looked at the details of hydration melting and ore metal introduction by fluids. However, there are a number of post-hydration phenomena that can occur during cooling. For example, one reviewer of this work (C. Jenkins) notes that Stillwater mine geologists describe the J-M Reef as being "top loaded" with more sulfide located in the upper parts of the Reef Package (within the anorthosites in particular). It is suggested that the eventual degassing of the hydrated assemblage on cooling resulted in the modest migration of the ore components upward only to reprecipitate them as they encounter fluid-undersaturated liquid in the overlying mush and is simply a continuation of the vapor-refining process that occurred in the footwall to the Reef described below.

Boudreau (1988) and Boudreau et al. (2019) have described a pothole-like transition from olivine-bearing rocks to gabbronorite along strike. Developed in the gabbronorite are both layer-parallel and cross cutting pipe-like pegmatoidal channels. Occurring in the core of some of these pegmatoids are decimeter-size bodies of massive sulfide. Further, the presence of soft sediment-like deformation/folds in the rocks immediately below the Reef suggest that the layering was not horizontal but tilted, allowing for a modest slumping. If so, then late fluids could move up-dip, resulting in the late loss of ore components from the olivine-bearing rocks and reprecipitating them in the developing pegmatoidal channelways in the adjoining gabbronorite.

Fluid as mineralizing agents in layered intrusions

Metal solubility considerations The ore component models developed here are by no means unique. However, the fluid compositions listed in Table 3 do illustrate the ore metal concentrations required to reproduce the ore grades as shown in Fig. 9. Ore grade is a simple function of the fluid/rock mass ratio; the higher this ratio while the rocks are sulfide saturated the lower the required fluid concentrations, especially for the PGE. While there is no debate that S and Cu can be readily remobilized, there is only recently been work suggesting that Ni and the PGE can be mobilized in significant quantities by high temperature fluids. As summarized by Le Vaillant et al. (2014), information on the aqueous speciation and thermodynamic properties of nickel and platinum group elements species is limited to common ligands such as chloride and bisulfide. For the PGE, the work of only a few studies have tried to understand the behavior of these metals and quantitatively model transport in hydrothermal fluids at the high temperature, upper crustal pressure conditions of mafic layered intrusions (e.g., Ballhaus et al. 1994; Sassani and Shock 1998; Hanley et al. 2005; Simon and Pettke 2009; Bell et al. 2009; Tagirov et al. 2013, 2019; Blaine et al. 2011; Scholten et al. 2018; Sullivan et al. 2022a, b; Simakin et al. 2021). Le Vaillant et al. also note that the data for high temperature Ni solubility is also limited, although hydrothermal Ni deposits associated with classic magmatic Ni–sulfide deposits such as the Sudbury are known (e.g., Tuba et al. 2013).

The Pt solubility runs of Sullivan et al. (2022a, b) done at 800–1000 °C at 200 MPa, $Cl_{total} = 32$ mol/kg H_2O, HCl/(HCl + NaCl) = 0.1 $f(O_2)$ = NNO-0.41 and extrapolated to the temperature of this study is about 28 ppm Pt, compares with 25 ppm required for the more favorable CO_2-rich case of this study. For Pd under similar conditions the solubility can exceed 300 ppm (Sullivan et al. 2022a), well in excess of the 75 ppm required from this study. Hanley et al. (2005) report similarly favorable results for Pt solubility in NaCl brines, and Simakin et al. (2021) report Pt solubility of 15–150 ppm in CO-CO_2 fluid at 950 °C. This, and the results of this study, suggest that a Cl- and CO_2-rich fluid is the more favorable fluid composition for metal transport and ore formation.

These PGE values are higher than is observed in Stillwater fluid inclusions reported by Hanley et al. (2005, 2008 and summarize in Table 3). However, the maximum estimated temperature they calculate is 700-715 °C or roughly 350 °C lower than the temperature implied by this study. The Pt and Pd concentrations of 0.4 to 4 ppm reported by Hanley et al. (2005) fall within the range of experimental studies of 1–15 ppm Pd at 700 °C reported by Hsu et al. (1991), suggesting that the fluid inclusions do not represent the PGE carrying potential at higher temperatures.

Fluid modeling by Mathez et al. (1989) in the C-O–H-Cl system suggested that the volatile phase initially would be an H_2O-poor, CO_2-CO-HCl mixture that evolved from supersolidus conditions (> 1000 °C) to more H_2O-rich compositions at lower temperatures. Because the CCO buffer crosses the more common oxygen buffers, the early fluid can become graphite saturated on cooling. Furthermore, Mathez and Webster (2005) suggested that these fluids would have been Cl-rich, consistent with the observed Cl-rich apatite compositions observed within and below the J-Reef. Regarding the fluid transport of the ore components, it is suggested that the early fluids were enriched in CO_2, HCl, the alkalis, sulfur and the ore metals, as this early fluid would be the first to remove the minor sulfide content from the footwall. The influx of later, more H_2O-rich but lower metal content fluids would be effective at partially remobilizing the earlier

precipitated sulfide. This high temperature remobilization can be modified by yet lower temperature alteration and serpentinization (e.g., Li and Ripley 2006).

Mass balance considerations Using the average J-M Reef grade and thickness noted above, if the source of the ore metals came from 1 km of underlying mush (to about the middle of the Bronzitite zone) the initial source rock concentration would need to average 20 ppb Pd and 6 ppb Pt *above* the currently observed background values to account for the metals in the reef. Metals supplied by 2 km of underlying section (to about the middle of the Peridotite zone) would halve these amounts. As noted by Sarah-Jane Barnes and co-investigators in a number of studies, the rocks below the J-M Reef (as well as those below the UG2 & Merensky Reef of the Bushveld complex) typically have PGE concentrations at or above presumed parent magma concentrations and are too high to represent trapped liquid component but also have bulk rock S concentrations below expected sulfide saturation concentrations (e.g., Barnes et al. 2009). The low bulk rock S/Se, the presence of magnetite rims on sulfide, and apparent replacement of sulfide with carbonates (Barnes et al. 2015; Aird et al. 2013, 2016) is some of the evidence the rock were initially sulfide-saturated but lost S to later degassing.

For the Stillwater Complex, Barnes et al. (2020) report an average of 52 ppm S, 19 ppb Pd and 25 ppb Pt for three N-I samples, and Barnes et al. (2015) similar values from the Ultramafic series. Keays et al. (212) report overall lower average background concentrations of 7 ppb Pd and 10 ppb Pt for the Peridotite zone up through GN-I with S decreasing from 100–200 to < 100 ppm. Using just the lower average background values reported by Keays et al. and the required metal abundance noted above, an ore fluid separating from the footwall would need to be 59–75% efficient at removing Pd and 23–38% efficient at removing Pt from 1–2 km of underlying mush. These numbers are broadly in agreement with the earlier estimates of Boudreau and McCallum (1992).

A question not fully addressed in orthomagmatic models is exactly how the initial high background values are attained. That is, conventional Raleigh fractionation assumes all the precipitated phases fully equilibrate with the entire magma mass. In such a case precipitation of ~ 0.05 wt.% sulfide (e.g., Aird 2016) as a fraction of the precipitate assemblage should rapidly deplete the magma given partition coefficients on the order of 10^4 or higher. In contrast, in situ fractionation (Langmuir 1989) envisions crystallization occurring only locally along the margins of the magma chamber in solidification fronts. In this case fractionation occurs by the return of an evolved interstitial liquid from the crystallization front back into the main magma body. The net effect for strongly incompatible elements is much the same as for Raleigh fractionation, as these elements always go with the residual liquid in both cases. The main difference is for compatible elements; for in situ crystallization any precipitating sulfide would only see the metal concentration of the crystallization front and hence the bulk concentration in the precipitated assemblage is that of the magma. Over time, the metal concentrations in the main magma body decrease owing to dilution of the evolved liquid returned from the crystallization front but not as rapidly as for Raleigh fractionation. For a sulfide-saturated magma containing 15 ppb Pd, the initial bulk mush will also contain 15 ppb but will increase as the residual liquid is lost. Assuming half the liquid is lost to compaction, then the bulk mush could roughly double (to 30 ppb Pd). Overall, in situ fractionation and frequent recharge events can produce a thick mush column that, absent vapor saturation and metal loss, can have bulk ore component concentrations as high or higher than the parent liquid.

Vapor refining of a solidifying mush The petrogenetic model proposed here suggests that the ore metals, originally enriched in a minor sulfide fraction in the footwall mush, are remobilized upward during degassing of interstitial liquid deeper in the crystal pile. PGE sulfides are reprecipitated when fluids encounter hotter, fluid undersaturated rocks and induce partial incongruent melting. Unlike vapor-saturation in a well-mixed magma chamber, where the compositional evolution of the fluid can be modeled as a simple fractionation process, the fluid evolution history of the degassing interstitial liquid in a layered intrusion is a non-trivial task. This is because fluid exsolved deep in the crystal pile can migrate upward and redissolve in interstitial liquids that have not yet become fluid saturated, enriching them in volatile and metal components they might not see otherwise. Indeed, it is such vapor-refining processes that have been used to explain the unusually Cl-rich nature of apatite in and below the J-M Reef (Boudreau and McCallum 1989).

Based on simple partitioning behavior used in a chromatographic transport model, Boudreau and Meurer (1999) noted that the fluid transport of sulfur, base metals, and the PGE is largely a function of dissolution and reprecipitation of a minor sulfide fraction during degassing of a crystal pile. This is because of the strong partitioning of these elements into a sulfide phase owing to the large partition coefficients compared with those for silicate minerals; once the sulfide is resorbed the fluid will be the next best host for the ore metals (one exception being for Ni for olivine-rich host rock). Although this study used a conservative vapor/liquid partition coefficient of 10 for all ore elements, they can be as high as 10^3 for Pt (Hanley et al. 2005). Field evidence for the wholesale transport of the sulfide fraction is seen in the small bodies of massive sulfide that occur in the cores of some pegmatoidal channels along the J-M Reef (e.g.,

Boudreau 1999a) and in sulfide-enriched pegmatoids below OB-I described above.

Details of how ore metals and halogens can move and fractionate during degassing of a solidifying crystal mush have been discussed by Boudreau and McCallum (1989, 1992), Boudreau and Meurer (1999) and Aird et al. (2016). Briefly, a mush initially formed by crystallization of a fluid-undersaturated magma and solidifying by the loss of heat out the bottom will eventually become fluid saturated at some depth within the pile (Fig. 11a). Over time this will result in a lower section of fully solidified rock overlain by a fluid-saturated zone that is enriched in the volatile (including Cl) and ore metal content lost from the lower solid portions of the crystal pile to degassing. Ore components can precipitate at the top of the vapor-saturated zone as fluid is resorbed in vapor-unsaturated interstitial liquids, much as

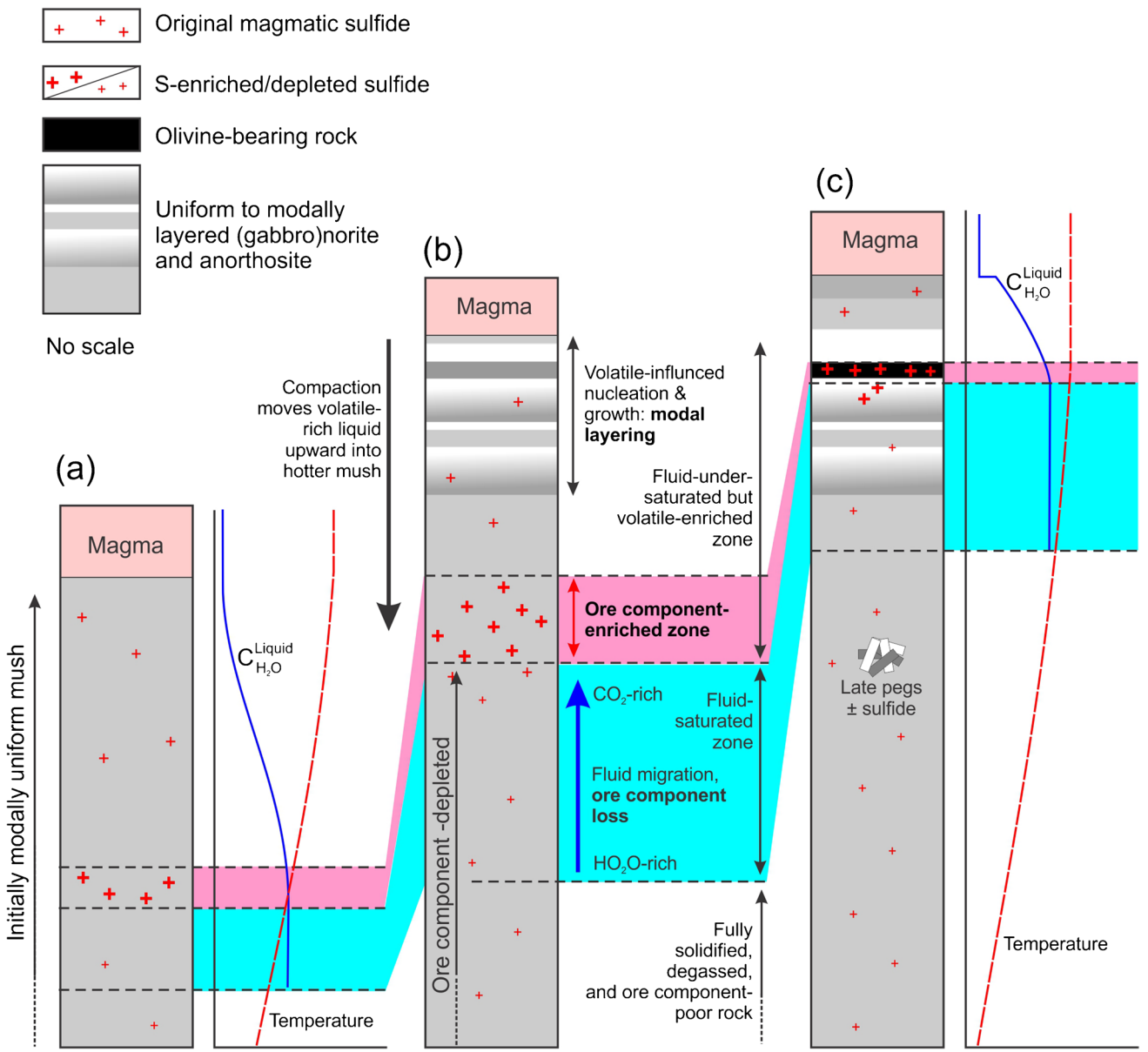

Fig. 11 Cartoon model of vapor refining model of a solidifying and degassing crystal mush that is losing heat out the bottom at three non-dimensional time steps a-c. **a** As the pile grows, fluid separating and moving upward from the deeper parts carries S and ore metals upward that are redeposited at higher levels where the interstitial liquid is not yet fluid-saturated. **b** Over time, this ore-element front becomes thicker as it contains all the volatile and ore components lost to degassing from the solidified part of the pile and moves closer to the top of the pile. **c** Eventually this front (and volatile-rich interstitial liquids moving upward by compaction) begins to affect magma crystallization, initially producing modal layering and eventual incongruent melting as the fluids and volatile-rich interstitial liquids encounter hotter rocks

is as described here. As the pile grows, this vapor-saturated zone becomes thicker and moves closer to the top of the crystal pile (Fig. 11b). Upward migration can be limited when either the fluid reaches the top of the crystal pile or reaches mush hot enough to induce substantial melting as modeled here (Fig. 11c). Loss of fluid to the main magma body after flux melting and sulfide precipitation can deplete the mush volatile budget as well. More broadly, the gain or loss of volatile species can lead to the development of modal layering by the "constitutional zone refining" process described by McBirney (1987). It is suggested that the increase in modal layering in the upper parts of GN-I and lower part of OB-I likely represents the early crystallization perturbations prior to the more extensive melting reactions as fluid input increased.

Conclusions

This work has shown that the observed olivine and plagioclase compositions and mineral modes of the troctolites and the pegmatitic peridotites of OB-I of the Stillwater Complex can be effectively modeled by the fluid-induced partial melting of norite, gabbronorite and melanorite protoliths. OB-I is a particularly good test case for this process as mineral stratigraphic trends do not strongly support the influx of compositionally distinct magmas for the re-appearance of olivine. More specifically, the compositional features are best modeled by the introduction of hydrothermal brines into hot, fluid-undersaturated assemblages as compared with simple pure H_2O hydration models. It is suggested that the presence of an interstitial plagioclase in olivine-rich rocks that is more albitic than expected can be a discriminant for poikilitic peridotite formed by hydration melting by a hydrothermal brine vs conventional magmatic interpretation as an olivine orthocumulate or heteradcumulate. Ore components can be introduced by the hydration event, with fluid/rock mass ratios of 0.25 for CO_2-rich fluids also broadly consistent with experimental solubilities for Pd and Pt.

The hydration melting explored in this study is but one of a range of fluid-mediated processes that can occur in layered intrusions. For example, it has been suggested that both layered and discordant anorthosites ± associated chromitites both in OB-I and in the Bushveld Complex are the result of leaching of mafic components by Cl-rich fluids as it move through hotter, fluid-saturated rocks (Maier et al. 2020; Marsh et al. 2021). The constitutional zone refining mechanism that can result in modal layering (McBirney 1987) is another. More broadly, the models suggest that PGE enrichment and associated changes in modal mineralogy can occur by processes occurring in a crystallizing magma/mush column without the need to call on unusual magma compositions.

The work done in this paper highlights the importance and need to continue research in experimental and theoretical petrology to high temperature hydrothermal fluids. Indeed, many thermodynamic databases have upper temperature limits for extrapolation of solution speciation equations that are below the sub-liquidus, upper crustal conditions appropriate for mafic intrusions (e.g., Dick 2019). While MELTS and PELE provide reasonable evidence for the hydration melting model, they lack the ability to model *true* fluid solution mixtures; MELTS modelling is restricted by reliable additions of H_2O and CO_2 only. There is need for more detailed experimental and theoretical work on volatile effects on mineral-melt relationships and mineral solubilities. For example, although Ni-NiO is a commonly used mineral buffer, Ni solubility experiments at the condition of this study are especially lacking. The same also applies to the other PGE besides Pd and Pt. A cleaver experimentalist could perhaps devise an experiment to test vapor-refining predictions. Finally, this study holds the potential to be applicable to olivine-bearing mineralized units in layered mafic intrusions all over the world (e.g., Scoon and De Klerk 1987).

Supplementary Information The online version contains supplementary material available at https://doi.org/10.1007/s00126-024-01267-2.

Acknowledgements This work was done as part of a Senior Thesis research project at Duke University by A.G. It was supported by Duke Undergraduate Research grants to A.G. Reviews by C. Jenkins and an anonymous reviewer are very much appreciated and led to substantial improvements.

Author contributions A.G. was responsible for the MELTS modeling and A.E.B. for the PELE modeling. Both shared in the writing.

Declarations

Neither author has any financial or non-financial interest that are directly or indirectly related to this work other than the selfless search for scientific truth. Indeed, being a student (A.G.) or retired (A.E.B.) neither author was even paid for this work.

References

Aird HM, Boudreau AE (2013) High-temperature carbonate minerals in the Stillwater Complex, Montana, USA. Contrib Mineral Petrol 166(4):1143–1160. https://doi.org/10.1007/s00410-013-0913-2

Ballhaus C, Ryan CG, Mernagh TP, Green DH (1994) The partitioning of Fe, Ni, Cu, Pt, and Au between sulfide, metal, and fluid phases: A pilot study. Geochim Cosmochim Acta 58(2):811–826. https://doi.org/10.1016/0016-7037(94)90507-x

Barnes SJ, Campbell IH (1988) Role of late magmatic fluids in Merensky-type platinum deposits: a discussion. Geology 16:488–491. https://doi.org/10.1130/0091-7613(1988)016%3c0488:ROLMFI%3e2.3.CO;2

Barnes SJ, Naldrett AJ (1985) Geochemistry of the J-M (Howland) Reef of the Stillwater Complex, Minneapolis Adit Area. I. Sulfide chemistry and sulfide-olivine equilibrium. Econ Geol 80:627–645

Barnes SJ, Naldrett AJ (1986) Geochemistry of the J-M Reef of the Stillwater Complex, Minneapolis Adit Area II. Silicate mineral chemistry and petrogenesis. J Petrol 27:791–825

Barnes S-J, Pagé P, Zientek ML (2020) The Lower Banded series of the Stillwater Complex, Montana: whole-rock lithophile, chalcophile, and platinum-group element distributions. Miner Deposita 55(1):163–186. https://doi.org/10.1007/s00126-019-00887-3

Barnes S-J, Pagé P, Prichard H M, Zientek ML, Fisher PC (2015) Chalcophile and platinum-group element distribution in the Ultramafic series of the Stillwater Complex, MT, USA—implications for processes enriching chromite layers in Os, Ir, Ru, and Rh. Miner Deposita 51(1):25–47. https://doi.org/10.1007/s00126-015-0587-y

Bell AS, Simon A, Guillong M (2009) Experimental constraints on Pt, Pd and Au partitioning and fractionation in silicate melt–sulfide–oxide–aqueous fluid systems at 800°C, 150MPa and variable sulfur fugacity. Geochim Cosmochim Acta 73(19):5778–5792. https://doi.org/10.1016/j.gca.2009.06.037

Blaine FA, Linnen RL, Holtz F, Bruegmann GE (2011) The effect of Cl on Pt solubility in haplobasaltic melt: Implications for micronugget formation and evidence for fluid transport of PGEs. Geochim Cosmochim Acta 75(24):7792–7805. https://doi.org/10.1016/j.gca.2011.10.010

Boudreau AE (1988) Investigations of the Stillwater Complex: Part IV. The role of volatiles in the petrogenesis of the J-M Reef. Minneapolis Audit Section Can Mineral 26:193–208

Boudreau AE (1999a) Fluid fluxing of cumulates: the J-M Reef and associated rocks of the Stillwater Complex, Montana. J Petrol 40(5):755–772. https://doi.org/10.1093/petroj/40.5.755

Boudreau AE (1999b) PELE—a version of the MELTS software program for the PC platform. Comp Geosci 25(2):201–203. https://doi.org/10.1016/s0098-3004(98)00117-4

Boudreau AE (2008) Modeling the Merensky Reef, Bushveld Complex, Republic of South Africa. Contrib Mineral Petrol 156(4):431–437

Boudreau AE (2016) The Stillwater Complex, Montana – overview and the significance of volatiles. Mineral Mag 80(4):585–637. https://doi.org/10.1180/minmag.2016.080.063

Boudreau AE, McCallum IS (1989) Investigations of the Stillwater Complex: Part V. Apatites as indicators of evolving fluid composition. Contrib Mineral Petrol 102:138–153

Boudreau AE, McCallum IS (1992) Concentration of platinum-group elements by magmatic fluids in layered intrusions. Econ Geol 87(7):1830–1848. https://doi.org/10.2113/gsecongeo.87.7.1830

Boudreau AE, Meurer WP (1999) Chromatographic separation of the platinum-group elements, gold, base metals and sulfur during degassing of a compacting and solidifying igneous crystal pile. Contrib Mineral Petrol 134(2–3):174–185. https://doi.org/10.1007/s004100050477

Boudreau AE, McCallum IS (1990) Low temperature alteration of REE-rich chlorapatite from the Stillwater Complex, Montana. Am Mineral 75:687–693

Boudreau AE, Mathez EA, McCallum IS (1986) The Halogen Geochemistry of the Stillwater and Bushveld Complexes: Evidence for Transport of the Platinum-Group Elements by Cl-Rich Fluids. J Petrol 27(4):967–986 Oxford University Press. https://doi.org/10.1093/petrology/27.4.967

Boudreau AE., Butak KC, Geraghty EP, Holick PA, Koski MS (2019) Mineral deposits of the Stillwater Complex. In MBMG Special Publication 122: Geology of Montana, vol. 1: Geologic History. (In press; available online at https://mbmg.mtech.edu/pdf/geologyvolume/BoudreauChapterFinal.pdf)

Braun K, Meurer W, Boudreau AE, McCallum IS (1994) Compositions of pegmatoids beneath the J-M Reef of the Stillwater Complex, Montana, U.S.A. Chem Geol 113(3-4):245–257. https://doi.org/10.1016/0009-2541(94)90069-8

Campbell IH, Naldrett AJ (1979) The Influence of silicate:sulfide ratios on the geochemistry of magmatic sulfides. Econ Geol 74(6):1503–1506. https://doi.org/10.1093/petrology/34.2.291

Dick JM (2019) CHNOSZ: Thermodynamic calculations and diagrams for geochemistry. Front Earth Sci 7. https://doi.org/10.3389/feart.2019.00180

Ford CE, Biggar GM, Humphries DJ, Wilson G, Dixon D, O'Hara MJ (1972) Role of water in the evolution of the lunar crust; an experimental study of sample 14310; an indication of lunar calc-alkaline volcanism. Lunar Planet Sci Conf Proc 3:207

Godel B, Barnes S-J (2008) Platinum-group elements in sulfide minerals and the whole rocks of the J-M Reef (Stillwater Complex): Implication for the formation of the reef. Chem Geol 248(3–4):272–294. https://doi.org/10.1016/j.chemgeo.2007.05.006

Gualda GAR, Ghiorso MS (2015) MELTS_Excel: A microsoft excel-based MELTS interface for research and teaching of magma properties and evolution. Geochem Geophys Geosys 16:315–324

Hanley JJ, Pettke T, Mungall JE, Spooner ETC (2005) The solubility of platinum and gold in NaCl brines at 1.5 kbar, 600 to 800°C: A laser ablation ICP-MS pilot study of synthetic fluid inclusions. Geochim Cosmochim Acta 69(10):2593–2611. https://doi.org/10.1016/j.gca.2004.11.005

Hanley JJ, Mungall JE, Pettke T, Spooner ETC, Bray CJ (2008) Fluid and halide melt inclusions of magmatic origin in the ultramafic and lower banded series, Stillwater Complex Montana, USA. J Petrol 49(6):1133–1160. https://doi.org/10.1093/petrology/egn020

Harper MP (2004) Platinum group element mineralizationin "Ballroom" of the J-M Reef of the Stillwater Complex, Montana. MS Thesis Brigham Young University 111

Helz RT (1976) Phase relations of basalts in their melting ranges at P H2O= 5 kb Part II Melt Compositions. J Petrol 17(2):139–193

Holloway JR, Burnham CW (1972) Melting relations of basalt with equilibrium water pressure less than total pressure. J Petrol 13(1):1–29

Hsu LC, Lechler PJ, Nelson JH (1991) Hydrothermal solubility of palladium in chloride solutions from 300 degrees to 700 degrees C; preliminary experimental results. Econ Geol 86(2):422–427. https://doi.org/10.2113/gsecongeo.86.2.422

Irvine TN, Keith DW, Todd SG (1983) The J-M platinum-palladium reef of the Stillwater Complex, Montana; II, Origin by double-diffusive convective magma mixing and implications for the Bushveld Complex. Econ Geol 78(7):1287–1334. https://doi.org/10.2113/gsecongeo.78.7.1287

Jenkins MC, Mungall JE, Zientek ML, Holick PA, Butak KC (2020) The nature and composition of the J-M Reef, Stillwater Complex, Montana, USA. Econ Geol 115(8):1799–1826. https://doi.org/10.5382/econgeo.4777

Jenkins MC, Mungall JE, Zientek ML, Costin G, Yao Z (2021) Origin of the J-M Reef and lower banded series, Stillwater Complex,

Montana, USA. Precambrian Res 367:106457. https://doi.org/10.1016/j.precamres.2021.106457
Jenkins MC, Mungall JE, Zientek ML, Butak KC, Corson SR, Holick PA, McKinley R, Lowers H (2022) The geochemical and textural transition between the reef package and its hanging wall, Stillwater Complex, Montana, USA. J Petrol 63(7). https://doi.org/10.1093/petrology/egac053
Keays RR, Lightfoot PC, Hamlyn PR (2012) Sulfide saturation history of the Stillwater Complex, Montana: chemostratigraphic variation in platinum group elements. Miner Deposita 47(1–2):151–173. https://doi.org/10.1007/s00126-011-0346-7
Labotka TC, Kath RL (2001) Petrogenesis of the contact-metamorphic rocks beneath the Stillwater Complex. Montana Geol Soc Am Bull 113(10):1312–1323. https://doi.org/10.1130/0016-7606(2001)113%3c1312:Potcmr%3e2.0.Co;2
Langmuir CH (1989) Geochemical Consequences of in situ crystallization. Nature 340:199–205
Latypov R (2019) Comment on "The Stillwater Complex: Integrating Zircon Geochronological and Geochemical Constraints on the Age, Emplacement History and Crystallization of a Large, Open-System Layered Intrusion" by Wall et al. (J Petrol, 59, 153–190, 2018). J Petrol 60(5):1095–1098. https://doi.org/10.1093/petrology/egz014
Latypov RM, Namur O, Bai Y et al (2023) Layered intrusions: Fundamentals, novel observations and concepts, and controversial issues. Earth Sci Rev. https://doi.org/10.1016/j.earscirev.2023.104653
Le Vaillant M, Fiorentini ML, Barnes SJ, Miller J (2014) Hydrothermal Footprints of Magmatic Nickel Sulfide Deposits. Mineral Res Inst W Australia 235
Li C, Ripley EM (2006) Formation of Pt-Fe alloy by desulfurization of Pt-Pd sulfide in the J-M Reef of the Stillwater Complex. Montana Can Mineral 44(4):895–903. https://doi.org/10.2113/gscanmin.44.4.895
Maier WD, Barnes S-J, Muir D, Savard D, Lahaye Y, Smith WD (2020) Formation of Bushveld anorthosite by reactive porous flow. Contrib Mineral Petrol 176(1):1–23. https://doi.org/10.1007/s00410-020-01760-7
Marsh JS, Pasecznyk MJ, Boudreau AE (2021) Formation of Chromitite seams and associated Anorthosites in layered intrusion by reactive volatile-rich fluid infiltration. J Petrol 62(2):1–23. https://doi.org/10.1093/petrology/egaa109
Mathez EA, Webster JD (2005) Partitioning behavior of chlorine and fluorine in the system apatite-silicate melt-fluid. Geochim Cosmochim Acta 69(5):1275–1286. https://doi.org/10.1016/j.gca.2004.08.035
Mathez EA, Kinzler RJ (2017) Metasomatic Chromitite seams in the Bushveld and Rum layered intrusions. Elements 13(6):397–402. https://doi.org/10.2138/gselements.13.6.397
Mathez EA, Dietrich VJ, Holloway JR, Boudreau AE (1989) Carbon Distribution in the Stillwater Complex and Evolution of Vapor During Crystallization of Stillwater and Bushveld Magmas (1989). Journal of Petrology 30(1):153–173. https://doi.org/10.1093/petrology/30.1.153
McBirney AR (1987) Constitutional zone refining of layered mafic intrusions. In: Parsons L (ed) Origins of Igneous Layering, NATO ASI Series C 186:437–452. https://doi.org/10.1007/978-94-017-509-5_13
McCallum IS, Raedeke LD, Mathez EA (1980) Investigations in the Stillwater Complex: Part I. Stratigraphy and structure of the Banded zone. Pp. 59–87 in: Irvine A, Dungan M (eds) The Jackson Volume. Am J Sci 280-A:59–87
McCallum IS (2011) The Stillwater Complex: A review of the geology. In: Cawthorn RG (ed) Layered Intrusions, Elsevier Science BV, pp. 441–483
McIlveen CL (1996) Anomalous platinum-group element occurrence below the JM Reef Stillwater Complex Montana. Dissertation, The University of Montana
Ripley EM, Wernette BW, Ayre A, Li C, Smith JM, Underwood BS, Keays RR (2017) Multiple S isotope studies of the Stillwater Complex and country rocks: An assessment of the role of crustal S in the origin of PGE enrichment found in the J-M Reef and related rocks. Geochim Cosmochim Acta 214:226–245. https://doi.org/10.1016/j.gca.2017.07.041
Rutherford MJ, Sigurdsson H, Carey S, Davis A (1985) The May 18, 1980, eruption of Mount St. Helens: 1. Melt composition and experimental phase equilibria. J Geophy Res 90(B4):2929–2947
Sassani DC, Shock EL (1998) Solubility and transport of platinum-group elements in supercritical fluids: summary and estimates of thermodynamic properties for ruthenium, rhodium, palladium, and platinum solids, aqueous ions, and complexes to 1000°C and 5 kbar. Geochim Cosmochim Acta 62(15):2643–2671. https://doi.org/10.1016/s0016-7037(98)00049-0
Scholten L, Watenphul A, Beermann O, Testemale D, Ames D, Schmidt C (2018) Nickel and platinum in high-temperature H_2O + HCl fluids: Implications for hydrothermal mobilization. Geochim Cosmochim Acta 224:187–199. https://doi.org/10.1016/j.gca.2018.01.005
Scoon RN, De Klerk WJ (1987) The relationship of olivine cumulates and mineralization to cyclic units in part of the upper Critical Zone of the Western Bushveld Complex. Can Mineral 25:51–77
Simakin A, Salova T, Borisova AY, Pokrovski GS, Shaposhnikova O, Tyutyunnik O, Bondarenko G, Nekrasov A, Isaenko SI (2021) Experimental study of Pt Solubility in the CO-CO_2 fluid at low fO_2 and subsolidus conditions of the ultramafic-mafic Intrusions. Minerals 11(2). https://doi.org/10.3390/min11020225
Simon AC, Pettke T (2009) Platinum solubility and partitioning in a felsic melt–vapor–brine assemblage. Geochim Cosmochim Acta 73(2):438–454. https://doi.org/10.1016/j.gca.2008.10.020
Sullivan NA, Zajacz Z, Brenan JM, Hinde JC, Tsay A, Yin Y (2022a) The solubility of gold and palladium in magmatic brines: Implications for PGE enrichment in mafic-ultramafic and porphyry environments. Geochim Et Cosmochim Acta 316:230–252. https://doi.org/10.1016/j.gca.2021.09.010
Sullivan NA, Zajacz Z, Brenan JM, Tsay A (2022b) The solubility of platinum in magmatic brines: Insights into the mobility of PGE in ore-forming environments. Geochim Cosmochim Acta 316:253–272. https://doi.org/10.1016/j.gca.2021.09.014
Tagirov BR, Baranova NN, Zotov AV, Akinfiev NN, Polotnyanko NA, Shikina ND, Koroleva LA, Shvarov YV, Bastrakov EN (2013) The speciation and transport of palladium in hydrothermal fluids: Experimental modeling and thermodynamic constraints. Geochim Cosmochim Acta 117:348–373. https://doi.org/10.1016/j.gca.2013.03.047
Tagirov BR, Filimonova ON, Trigub AL, Akinfiev NN, Nickolsky MS, Kvashnina KO, Chareev DA, Zotov AV (2019) Platinum transport in chloride-bearing fluids and melts: Insights from in situ X-ray absorption spectroscopy and thermodynamic modeling. Geochim Cosmochim Acta 254:86–101. https://doi.org/10.1016/j.gca.2019.03.023
Thomson JA (2008) Beneath the Stillwater Complex: Petrology and geochemistry of quartz-plagioclase-cordierite (or garnet)-orthopyroxene-biotite spinel hornfels, Mountain view area. Montana American Mineralogist 93(2–3):438–450. https://doi.org/10.2138/am.2008.2572
Todd SG, Keith DW, LeRoy LW, Shissel DJ, Mann EL, Irvine TN (1982) The J-M platinum-palladium reef of the Stillwater Complex, Montana: I. Stratigraphy and petrology. Econ Geol 77:1454–1480

Tuba G, Molnár F, Ames DE, Péntek A, Watkinson DH, Jones PC (2013) Multi-stage hydrothermal processes involved in "low-sulfide" Cu(–Ni)–PGE mineralization in the footwall of the Sudbury Igneous Complex (Canada): Amy Lake PGE zone. East Range Mineral Deposita 49(1):7–47. https://doi.org/10.1007/s00126-013-0468-1

Veksler IV Hou T (2020) Experimental study on the effects of H2O upon crystallization in the Lower and Critical Zones of the Bushveld Complex with an emphasis on chromitite formation. Contrib Mineral Petrol 175. https://doi.org/10.1007/s00410-020-01733-w

Wall CJ, Scoates JS, Weis D, Friedman RM, Amini M, Meurer WP (2018) The Stillwater Complex: Integrating Zircon Geochronological and Geochemical Constraints on the Age, Emplacement History and Crystallization of a Large, Open-System Layered Intrusion. J Petrol 59(1):153–190. https://doi.org/10.1093/petrology/egy024

Waters C, Boudreau AE (1996) A reevaluation of crystal-size distributions in chromite cumulates. Am Mineral 81(11–12):1452–1459. https://doi.org/10.2138/am-1996-11-1217

Zientek ML, Cooper RL, Corson SR, Geraghty EP (2002) Platinum-group element mineralization in the Stillwater Complex, Montana. In: The geology, geochemistry, mineralogy and mineral beneficiation of platinum-group elements, Can Inst Mining and Metallurgy, pp 459–481